NASA Contractor Report 4558

A Parametric Study of Harmonic Rotor Hub Loads

Chengjian He
Lockheed Engineering & Sciences Company
Hampton, Virginia

Prepared for
Langley Research Center
under Contract NAS1-19000

National Aeronautics and
Space Administration
Office of Management
Scientific and Technical
Information Program
1993

CONTENTS

LIST OF TABLES

LIST OF FIGURES

Summary

This report presents a parametric study of vibratory rotor hub loads in a nonrotating system. The study is based on a CAMRAD/JA model constructed for the "growth" version of the U.S. Army's UH-60A Black Hawk helicopter (GBH). The GBH is a Mach-scaled wind tunnel rotor model with high blade twist ($-16°$). The theoretical hub load predictions are validated by correlation with available measured data. Effects of various blade aeroelastic design changes on the harmonic nonrotating frame hub loads at both low and high forward flight speeds are investigated. The study aims to illustrate some of the physical mechanisms for change in the harmonic rotor hub loads due to blade design variations.

Nomenclature

EI_{zz}	flapwise bending stiffness, $lbf\text{-}ft^2$
EI_{xx}	chordwise bending stiffness, $lbf\text{-}ft^2$
F_x, F_y, F_z	4P harmonic hub forces in nonrotating frame, lbs
GJ	torsional stiffness, $lbf\text{-}ft^2$
M_x, M_y, M_z	4P harmonic hub moments in nonrotating frame, $ft\text{-}lbs$
p_k, q_k	generalized coordinates of blade torsion and bending
R	rotor radius, ft
r	blade radial coordinate, nondimensionalized on R
μ	advance ratio
ψ	rotor azimuth
Ω	rotor rotational speed, rad/sec
$(\dot{})$	derivative with respect to time

Introduction

Rotorcraft vibration reduction is a challenge that is receiving the continuous attention of rotorcraft researchers, Refs [1-15]. Among various efforts to reduce the vibration

(absorbers, isolators, active blade control, etc.), a blade design for low vibration is an especially attractive approach since it deals with the problem in early design stages which is cost effective.

A rotorcraft is a complicated dynamic system. The flexible rotor blades encounter harmonic variations of the relative wind during their rotation in forward flight. Rotor aeroelastic response generates vibratory hub loads which pass to the nonrotating frame in harmonics that are a multiple of the number of rotor blades, given that there is no dissimilarity between blades. Among all other vibration excitation sources (tail rotor, impingement of rotor downwash on airframe, transmission, etc.), these harmonic hub loads contribute most significantly to the vehicle vibration. An understanding of the variation of the vibratory hub loads with design change is valuable as a guide for the design of low vibration rotorcraft.

There are works on the topic of sensitivity of vibratory hub loads to variations in blade parameters, Refs. [16-18]. These studies have enriched the design guideline for low vibration blades. In this report, a comprehensive rotorcraft analysis program (CAMRAD/JA), Ref. [19], is applied to investigate aeroelastic tailoring of an advanced rotor blade (GBH). This baseline blade was designed with an advanced aerodynamic approach. It is both tapered and twisted. The blade twist is as high as $-16°$ which is much higher than conventional blades ($-8°$, in general). The blade also has three different sets of airfoils distributed along the span for improved aerodynamic performance. It is intended that a parametric study of harmonic hub loads can provide some insight into the dynamic behavior of this aerodynamically advanced rotor. The investigation is made concerning the effect of blade twist, center-of-gravity offset, aerodynamic center offset from the elastic axis, mass and stiffness variation. The influence of altering design parameters on harmonic hub loads is investigated in both low and high speed flight since these are two high vibration regions. Where measured data are available, analytical results are compared to verify the theoretical predictions.

Wind Tunnel Model Rotor Description

The baseline model rotor investigated in this study is a 1/6-size, Mach-scaled representation of the "growth" version of the U.S. Army's UH-60A Black Hawk helicopter rotor, Ref. [12]. It is a four-bladed articulated rotor with coincident flap and lead-lag hinges. There is a pitch-flap coupling ratio measured as 0.5.

The baseline rotor blades are tapered with a $-16°$ linear twist, Fig. 1. The blades use the RC(4)-10, RC(3)-10, and RC(3)-08 airfoils, Refs. [20-21]. The RC(3)-10 and RC(3)-08 are utilized to improve airfoil performance under compressibility effect and the RC(4)-10 for airfoil stall behavior. The chordwise center-of-gravity, aerodynamic center, and elastic axis were coincident and located at the blade quarter-chord. The detailed blade mass and stiffness properties are listed in Ref. [12].

Analytical Rotor Modeling

A formulation of the rotor hub loads problem should address three essential aspects (i.e., elastically deformed rotor blades, airloads exciting the blade dynamics and influence of blade shed and trailing vorticity on the airloads). The system equations thus formed are, in general, nonlinear and with periodic time-varying coefficients in forward flight. These system equations can be solved with various integration schemes, or through harmonic balance with rotor rotational speed as the fundamental harmonic, or by a periodic shooting method. The solution attained is associated with a specific set of rotor control pitch. For a given flight condition, the blade pitch setting is adjusted until the given flight condition is satisfied which is conventionally called the vehicle trim process.

Rotor-fuselage interaction is another important issue for the vibratory load prediction. But, this study is based on a wind tunnel rotor model with a fixed rotor hub. The model constructed from CAMRAD/JA is for an isolated rotor only.

Blade Dynamics

The structural model of the rotor blade for CAMRAD/JA is based on the engi-

Table 1: Natural frequencies (1/rev) of coupled flap-lag modes

Modes	1st	2nd	3rd	4th	5th
calculated	0.312	1.045	2.890	5.439	6.695
measured			2.855	5.339	6.481

neering beam theory which assumes that the plane normal to the elastic axis remains a plane, Ref. [19]. This is normally well satisfied for an isotropic rotor blade with a high aspect ratio. The structural model of CAMRAD/JA includes only the lowest order terms. Nonlinear effects are accounted for in the inertial and aerodynamic forces. CAMRAD/JA solves for the blade dynamic response in the modal domain. The blade is assumed to deform in both flapwise and chordwise directions. The flap and lead-lag of the blade motions are coupled in the modal calculation. The blade torsion modes are solved independently. The equations of motion for bending and torsion are, however, coupled in both airloads and inertial loads analysis.

$$\left[M \right] \left\{ \begin{array}{c} \ddot{q}_k \\ \ddot{p}_k \end{array} \right\} + \left[C \right] \left\{ \begin{array}{c} \dot{q}_k \\ \dot{p}_k \end{array} \right\} + \left[K \right] \left\{ \begin{array}{c} q_k \\ p_k \end{array} \right\} = \left\{ F \right\} + \left\{ \begin{array}{c} F_{ae} \\ M_{ae} \end{array} \right\} \qquad (1)$$

where q_k and p_k are the generalized coordinates for blade bending and torsion, respectively. The F are generalized non-aerodynamic forces, and F_{ae} and M_{ae} are generalized aerodynamic forces.

The calculated blade natural frequencies at a typical collective pitch (6°) in the analysis are presented in Table 1. It is customary in rotorcraft dynamics to use the 1/rev (or 1Ω) to present blade frequencies. The rotor rotational speed is 69.32 rad/sec (662 rpm) for this study. There are five coupled flap-lag modes. The first mode is for rigid lag. The second mode is rigid flap. The third and fourth are elastic flap dominated, and the fifth is mainly of elastic lag motion.

Up to five coupled flap-lag modes are retained for blade dynamic response analysis. These modes cover a frequency range from 0.3 to 6.70/rev. The calculated elastic mode (3rd to 5th) frequencies are compared with experimentally measured values in Table 1. They are in close agreement. Since the following higher bending mode has a

natural frequency of 9.15/rev, the five coupled flap-lag modes used here are believed to be sufficient for 4P vibratory loads analysis. One elastic torsion mode is used that has a frequency of 4.924/rev. The rigid pitch motion due to control link flexibility is also included. The truncation of the torsional modes are justified as the frequency of the immediate next higher torsional mode is at 14.37/rev. The validation of the mode choice is presented in later section of the paper.

Rotor Aerodynamics

In forward flight, a rotor blade encounters 1/rev variation in velocity tangential to its rotational plane. This comes together with highly nonuniform and rapid variation of induced flow normal to the blade due to rotor vortex wake. They are responsible for harmonic airloads, the excitation forces for rotor vibration. Dynamic stall of the rotor blade during high speed forward flight or maneuvering of helicopters is another source of vibratory airload. The dynamic stall, however, is not modeled in this study since it is not a concern of all the cases investigated.

Therefore, the rotor vortex wake is a primary modeling issue for the harmonic rotor hub load calculation. CAMRAD/JA calculates rotor airloads using blade element theory, Ref. [19]. The analysis of airfoil two-dimensional aerodynamic characteristics is modified to account for the effects of reverse flow, yawed flow, and blade tip flow. The rotor three-dimensional nonuniform induced inflow is calculated using a vortex wake model. Both prescribed and free (distorted) wakes have been investigated. CAMRAD/JA models the wake as near wake, rolling up wake, and far wake. The near wake includes both trailed and shed vorticity. The rolling up wake describes rolling up process of the trailing vorticity. The details of the roll-up process, such as the starting location of the roll-up, the strength of the tip vortex, and the vortex core radius, are modeled, not calculated. The far wake models the rolled-up tip vortex. The GBH rotor blades have a high negative twist (-16 degrees). This results in negative loading at the advancing blade tip. Therefore, a model with double circulation peaks is employed by CAMRAD/JA to allow proper modeling of the negative tip loading.

Trim Solution

There are two tasks involved in the trim solution for the harmonic rotor hub loads calculation. First, the blade pitch control required for a specified flight condition is calculated. Then, a periodic rotor response is solved for the control applied. It is, in fact, an iterative process where both the control satisfying the flight state and periodicity of rotor response associated with the control are converged.

The blade pitch control applied to achieve the specified flight condition is computed with the Newton-Raphson method. For the GBH rotor test case, the wind tunnel trim is utilized with rotor thrust, rotor drag, and the tip-path-plane orientation as the trim target. Thus, the corresponding trim variables are rotor collective pitch, longitudinal and lateral cyclic pitch, and rotor shaft angle. The shaft angle is added as a trim variable for consideration of forward flight influence.

The periodic motion for the applied blade pitch control is calculated using the harmonic balance method. The integration of the rotor equations of motion advances around the rotor azimuth, calculating the forcing function in the time-domain and then updating the harmonics of the motion at each time step. The harmonic rotor hub loads are obtained when both rotor control and periodicity of rotor motion are converged.

Validation of the Analytical Model

The first results are attained for 4P vertical shear of the baseline GBH rotor model. The harmonic vertical shear are calculated for a thrust solidity ratio of $C_T/\sigma = 0.058$ at various advance ratios. The rotor is trimmed such that there is no first harmonic flapping with respect to the shaft. With a prescribed wake model, the variation of the 4P vertical shear with advance ratio follows the trend of measured data, Fig. 2. They both show the peaks at both high and low flight speed. The 4P vertical shear between the predicted and wind tunnel measured data are fairly well correlated. The 4P roll and pitch moments at fixed system (21 inches below the rotor hub) have also been compared to the measured data, Figs. 3-4. There are correlations between the predicted and the measured. The predicted trends agree well with the measured data. Some discrepancy

occurs at low speed ($\mu = 0.10$) with the prescribed wake model. A distorted free wake provides improvement, Fig. 5. The free wake model improves the prediction at low forward flight speed in its ability to model the highly-distorted rotor wake at the low speed. It does, however, often present a solution convergence problem. It has also a larger error at the cruise speed (around $\mu = 0.20$), Fig. 5. To further illustrate the importance of using an appropriate wake model in harmonic rotor hub load calculation, Fig. 6 compares the results from three different wake models. The double circulation peak model was designed for application to the case with negative tip loadings, Ref. [19]. For this highly twisted blade ($-16°$), there exists a negative aerodynamic loading around the advancing tip region under the flight conditions investigated. As shown in Fig. 6, this double peak modeling captures the physical behavior of the wake and improves the prediction significantly as compared to the conventional single peak model. Fig. 6 also presents the results from linear inflow modeling of Coleman and Feingold, Ref. [22]. This linear inflow model neglects both the higher harmonic variation and higher order radial distribution of the induced inflow which are major excitation sources of rotor vibration. It is obvious from the figure that the linear inflow model can provide no accurate hub vibratory load information.

The effect of structural dynamics on harmonic hub loads is presented in Fig. 7. The results from three modelings are shown. The basic modeling has five coupled flap-lag modes and one elastic torsion mode (plus a rigid blade pitch motion) as discussed in the previous section ("Analytical Rotor Modeling"). The second modeling adds one more higher bending mode (9.15/rev); the last one adds both the higher bending and a higher torsion mode (14.37/rev). As seen from the figure, the results show very minor difference from adding higher structural modes. This indicates that the basic blade structural dynamics model used in this study is sufficient.

Parametric Study of Aeroelastic Tailoring

A parametric study is performed on the GBH model rotor to investigate the effect of rotor aeroelastic tailoring on harmonic rotor hub loads. The blade variables include

the blade twist, the offset of both chordwise center-of-gravity (c.g.) and aerodynamic center (a.c.) from the elastic axis, nonstructural mass placement, and blade bending and torsional stiffness distributions.

The vibratory rotor hub loads in a nonrotating frame are obtained from the summation of the rotor hub reactions over each blade in the rotating frame. Based on the sum of harmonics, for a four-bladed rotor in a steady periodic response, 3P and 5P in-plane root shears of each rotating blade are passed to the nonrotating frame as a 4P vibratory longitudinal force (F_x) and side force (F_y). Similarly, only 3P and 5P root moments contribute to the 4P roll (M_x) and pitch (M_y) moments at the nonrotating frame. The 4P vertical shear F_z and yaw moment M_z result from 4P loads in the rotating frame.

Effect of Twist

It is known that blade twist is used to lower rotor power required to improve its aerodynamic performance. This improvement is achieved by redistributing spanwise blade load to reduce both rotor induced and profile drag. Figure 8 shows spanwise distribution of blade sectional normal force for three differently twisted blades under the same trim condition. The more twisted blade has a lighter loading at the tip region. The tip loading with high twist ($-12°$ and $-16°$) even becomes negative. Fig. 8 presents the blade normal loading at advancing azimuthal location ($\psi = 90°$). Similar trends exist for the spanwise variation of blade loadings for other rotor azimuthal locations.

The twist also increases the blade flap-lag coupling. Among all the five coupled flap-lag modes, a significant increase in flap-lag coupling occurs with the fifth mode which is dominated by an in-plane lead-lag motion. Increased twist adds a significant amount of flapping motion to this mode, Fig. 9.

Although there is no change in the frequency and mode shape of the torsional mode due to the blade twist, the blade torsional response is affected by the twist, Fig. 10. The larger twist causes a greater blade torsional response which compensates blade pitch control for a given trim condition.

These changes due to the twist result in an unfavorable impact of high twist on vibratory rotor hub loads. Figure 11 shows the hub loads for these different twisted

configurations at $\mu = 0.30$. All components of the 4P vibratory hub loads, except the pitch moment, increase with the blade twist. The largest increase occurs in 4P vertical shear and yaw moment. The twist effect on harmonic hub loads at low flight speed ($\mu = 0.10$) is presented in Fig. 12, the same trend is seen.

Effect of Chordwise C.G. Offset

For prevention of classical bending-torsion flutter, it is beneficial for the chordwise center-of-gravity (c.g.) to be forward of the elastic axis. For blade dynamic response, the effective c.g. offset is proportional to the mass weighted bending-torsion coupling. To examine the effect on harmonic hub loads of the chordwise c.g. offset, the c.g. is moved 10% of the chord length forward of and aft of the elastic axis along the blade radial stations from $0.40R$ to $0.50R$. The former is denoted as "CG45(+)", while the latter is "CG45(-)". These two cases correspond to the anti-node region of the third blade flap-lag mode. As mentioned, the baseline blade has a coincidence of chordwise center-of-gravity, aerodynamic center, and elastic axis.

The results in Figs. 13-14 show that moving the chordwise c.g. forward of the elastic axis results in lower vibratory loads than that of placing the c.g. aft of the elastic axis. This is due to the flap-torsion inertial coupling effect that causes a phase change in blade torsional response shown in Figs. 15-16. The torsional response for the c.g. forward of the elastic axis oscillates out-of-phase with the case when the c.g. is aft of the elastic axis. This explains why the c.g. movement across the elastic axis affects the harmonic hub loads differently. A chordwise c.g. located forward of the elastic axis has an advantage for lower vibratory hub loads.

A chordwise c.g. offset movement has also been investigated at blade stations from $0.6R$ to $0.7R$ which are related to the anti-node region of the 4th coupled flap-lag mode. A similar trend exists with only a minor difference in the in-plane shears as compared to the previous cases.

Effect of Aerodynamic Center Offset

The offset of aerodynamic center (a.c.) from the elastic axis could be, in fact,

realized by adjusting chordwise location of the blade section twist center. The influence of aerodynamic center movement on harmonic hub loads is caused by a change in blade torsional response due to sectional aerodynamic pitching moment. For this study, the aerodynamic center at $0.6R$ to $0.7R$ blade stations are moved 10% of the chord length forward (denoted as "AC67(+)") or after (denoted as "AC67(-)") the elastic axis to examine the effect on harmonic hub loads.

Figures 17-18 compare the harmonic hub loads for these two modifications with the baseline configuration. The aerodynamic center located after the elastic axis is, in general, beneficial to vibratory loads reduction for both high ($\mu = 0.3$) and low ($\mu = 0.10$) forward flight speed. There are exceptions for longitudinal force (F_x) and rolling moment (M_x) at $\mu = 0.3$ and pitching moment (M_y) at $\mu = 0.10$. Unlike the effect of chordwise c.g. offset, the aerodynamic center offset mainly changes the mean of the blade torsional response and not the phase shift as shown in Figs. 19-20.

Effect of Addition of Mass

Mass tuning is another way to reduce rotor vibration. Adding nonstructural masses alters both blade natural frequencies and mode shapes, and thus affects the blade dynamic response.

In this investigation, the effect of masses added at three different blade spanwise locations are examined and compared to experimentally measured data from Ref. [12]. For comparison, the same amount of concentrated mass as in the experiment is placed at $0.30R$, $0.50R$, and $0.85R$ radial locations, respectively. For identification, these configurations with added mass are denoted as "M30", "M50", and "M85" accordingly. The mass weighs 0.00838 slug and represents 8.7% of total blade mass. Table 2 shows the influence of the added mass on natural frequencies of coupled flap-lag modes. There is no effect of the added mass on the torsion modes.

It is noted that mass added at 0.30R lowers the natural frequencies of all three elastic modes (3rd to 5th modes). This is due to the fact that the mass added inboard increases the modal mass. This added mass has little effect on the first two

Table 2: Variation of blade frequencies with added mass

Modes	1st	2nd	3rd	4th	5th
Baseline	0.312	1.045	2.890	5.439	6.695
M30	0.315	1.045	2.778	5.186	6.354
M50	0.314	1.046	2.778	5.467	6.419
M85	0.256	1.030	2.944	5.512	6.297

rigid blade modes. The mass placed at 0.50R has a similar effect except for the 4th mode frequency. The mass placed at 0.85R, however, increases the 3rd and 4th mode frequencies because of dominant centrifugal stiffening effect outboard and decreases the first lag mode frequency due to the increased modal mass.

The blade elastic mode shapes are strongly affected by the addition of masses. The changes of mode shapes directly alter the modal generalized forces. Figure 21 presents the generalized force variation for the third flap-lag mode. Both "M30" and "M50" configurations have a smaller magnitude of the forcing function than the baseline, whereas "M85" configuration stays nearly the same mean magnitude. From a harmonic analysis, it is found that "M30" and "M50" modifications create a phase shift in the third harmonic component of the generalized force. The effect of these additional masses on the generalized force of the fourth mode is shown in Fig. 22. Also based on the results from a harmonic analysis, the "M85" modification causes a smaller amplitude of the third harmonic, a phase shift in the fourth harmonic of the generalized force and a much smaller mean magnitude also. The "M30" lowers the mean magnitude of the generalized force. The effects of the "M50" is not significant on this mode. The fifth mode is a strongly coupled flap-lag motion. The "M30" modification decreases the mean magnitude of the generalized force related to its flapping component and causes a phase shift in its fifth harmonic, Fig. 23. The magnitude of the forcing function associated with the lag motion component of the fifth mode is decreased by the "M30" modification, Fig. 24. The "M50" has a similar effect as the "M30" on the fifth mode except there is no large phase shift. The "M85" configuration mainly affects the phase

Table 3: Variation of blade frequencies with flapwise stiffness

Modes	1st	2nd	3rd	4th	5th
Baseline	0.312	1.045	2.890	5.439	6.695
EIzz(+)	0.312	1.045	2.913	5.455	6.696
EIzz(-)	0.312	1.045	2.863	5.418	6.693

of 4th and 5th harmonic of the generalized force for the lag motion of the fifth mode. It also increases the mean magnitude of the flap component of the generalized force.

Figures 25-26 show the impact of mass tuning on 4P hub loads. Among three different mass placements, the mass placed at $0.50R$ reduces all six components of harmonic hub loads simultaneously at $\mu = 0.30$. It has the same effect at $\mu = 0.10$ except for the pitching moment (M_y). The mass placed at 0.85R reduces the 4P shears, but increases the roll and pitch moments significantly. The effect of adding mass at $0.3R$ results in a slight increase of most vibratory load components at $\mu = 0.30$, but reduces vibratory loads at $\mu = 0.10$. The experimental data available for validation are the 4P vertical shear measurement. These wind tunnel measured data are presented in Fig. 27. The trend of mass tuning effect agrees well with the analytical prediction.

Effect of Flapwise Bending Stiffness

Within the limit of satisfying blade strength requirements, a low harmonic hub load may also be obtained through an appropriate blade stiffness distribution. Two cases are tested to investigate the effect on harmonic hub loads of blade flapwise bending stiffness. The blade flapwise bending stiffness is varied for $\pm 20\%$ at 0.4R to 0.6R locations which correspond to maximum flapwise bending curvature of the third mode. These two cases are denoted as "EIzz(+)" and "EIzz(-)" respectively.

The results show very minor change of blade natural frequencies, Table 3. Both blade natural frequencies and mode shapes are not as sensitive to the flapwise stiffness perturbation as for the cases of mass tuning. The same amount of change in flapwise bending stiffness at $0.7R$ to $0.8R$ locations, where the maximum bending curvature of

the 4th mode is located, is also investigated. Only minor change in blade dynamic characteristics occurs. This may be due to the fact that centrifugal stiffness affects blade bending behavior more than the flapwise stiffness.

There are, however, aeroelastic coupling effect due to the flapwise bending stiffness perturbation. This can be seen in Fig. 28. For the case of $\mu = 0.30$, lowering the stiffness alters the flapwise component of generalized force of the third mode. This results in an increase of 4P hub side force (F_x) and rolling moment (M_x) , Fig. 29. For the low flight speed case ($\mu = 0.10$), both increase or decrease of the bending stiffness influence the generalized force, Fig. 30. The changes, however, mainly occur at first quadrant of the rotor disk which implies a coupling with the rotor wake effect. This results in a 4P shear reduction from lowering the bending stiffness, Fig. 31. Also, F_z and M_z are both reduced from an increase or decrease of the bending stiffness.

Effect of Chordwise Bending Stiffness

The chordwise bending stiffness along $0.4R$ to $0.6R$ radial stations is changed by $\pm 20\%$ to investigate its effect on harmonic hub loads, denoted as "EIxx(+)" and "EIxx(-)", respectively. The $0.4R$ to $0.6R$ locations correspond to maximum chordwise bending curvature of the fifth mode and maximum flapwise bending curvature of the third mode also.

For $\mu = 0.30$, there is no remarkable change in harmonic rotor hub loads from this chordwise bending stiffness modification. It does, however, show the reduction trend of in-plane shears (F_x and F_y) and yaw moment (M_z) from lowering chordwise bending stiffness, Fig. 32. The trend is, however, different for $\mu = 0.10$, Fig. 33. This is explained by the coupling with the wake effect as indicated in Fig. 34. The figure shows a change of the generalized force of the third bending mode in the first quadrant of the rotor disk. This change only exists with the low speed case ($\mu = 0.10$), where the wake effect is significant. For the high speed case ($\mu = 0.30$), there is not this type of change from the perturbation of the chordwise bending stiffness.

Effect of Torsion Stiffness Variation

The torsional stiffness from 0.3R to 0.8R radial stations is increased or decreased by 20% to investigate its influence on vibratory hub loads. These two cases are denoted as "GJ(+)" and "GJ(-)", respectively.

The change of blade torsional stiffness results in a shift of the natural frequency of the first blade elastic torsional mode. Increasing torsional stiffness raises the frequency from 4.924/rev to 5.208/rev, whereas decreasing the torsional stiffness lowers the frequency to 4.759 /rev. Their effect on harmonic hub loads are different, Figs. 35-36. For this model rotor, decreasing torsional stiffness is beneficial to the reduction of harmonic shears and rolling moment, but not the pitching moment at low speed. Increasing torsional stiffness increases shear and rolling moment at higher speed.

Conclusions

A parametric study of vibratory rotor hub loads has been performed on an aerodynamically advanced model rotor which has a various airfoil distribution and a high blade twist. The following conclusions can be made from this investigation.

1. A higher blade twist results in a higher rotor vibration.

2. Altering the torsional response is effective for vibration reduction.

3. Accepting a weight penalty, mass tuning is also effective.

4. Bending stiffness modification for vibration reduction is less effective.

5. It seems there is no single method to reduce all six components of vibratory hub loads simultaneously by a significant amount. Different design variables (both aerodynamic and structural dynamic parameters) need to be appropriately combined to achieve overall vibration reduction.

References

1. Flannelly, W.G.,"The Dynamic Anti-resonant Vibration Isolator," Proceedings of the 22nd Annual National Forum of the American Helicopter Society, Washington, D.C., May 1966.

2. Hamouda, N.H., and Pierce, G.A.,"Helicopter Vibration suppression Using Simple Pendulum Absorbers on the Rotor Blade," American Helicopter Society Northeast Region National Specialists' Meeting on Helicopter Vibration, Hartford, Connecticut, Nov. 1981.

3. McHugh, F.J. and Shaw, J., Jr., "Helicopter Vibration Reduction with Higher Harmonic Blade Pitch," Proceedings of the Third European Rotorcraft and Powered-Lift Aircraft Forum, Paper No. 22, Sept., 1977.

4. Wood, E.R., Powers, R.W., Cline, J.H. and Hammond, C.E.,"On Developing and Flight Testing a Higher Harmonic control System," Journal of the American Helicopter Society, Vol. 22, No.1, Jan. 1985.

5. Friedmann, P. P. and Shanthakumaran, P., "Optimum Design of Rotor Blades for Vibration Reduction," *Journal of the American Helicopter Society*, Vol. 29(4), Oct. 1984, pp. 70-80.

6. Yen, J.G.,"Coupled Aeroelastic Hub Loads Reduction," AHS/NAI International Seminar, Nanjing, China, Nov. 1985.

7. Peters, D. A., Rossow, M. P., Korn, A., and Ko, T., "Design of Helicopter Rotor Blades for Optimum Dynamic Characteristics," *Computers and Mathematics with Applications*, Vol. 12(1), 1986, pp. 85-109.

8. Weller, W. H. and David, M. W., "Experimental Verification of Helicopter Blade Design Optimization for Minimum Vibration, Proceedings of the 44th Annual National Forum of the American Helicopter Society, Washington, D.C., June 1988.

9. Lim, J. W. and Chopra, I., "Aeroelastic Optimization of a Helicopter Rotor," *Journal of the American Helicopter Society*, Vol. 34(1), Jan. 1989, pp. 52-62.

10. Pritchard, J. and Adelman, H., "Optimal Placement of Tuning Masses for Vibration Reduction in Helicopter Rotor Blades," AIAA Journal, Vol. 28, No. 2, Feb. 1990, pp. 309-315.

11. Chattopadhyay, A. and Chiu, Y. D., "An Enhanced Integrated Aerodynamic Load/Dynamic Approach to Optimum Rotor Blade Design," Proceedings of the 46th Annual Forum of American Helicopter Society, Washington D.C., June 1990, pp. 459-468.

12. Matthew L. Wilbur,"Experimental Investigation of Helicopter Vibration Reduction Using Rotor Blade Aeroelastic Tailoring," Proceedings of the 47th Annual Forum of the American Helicopter Society, Phoenix, Arizona, May 1991.

13. D.K. Young and F.J. Tarzanin Jr., "Structural Optimization and Mach Scale Test Validation," Proceedings of the 47th Annual Forum of the American Helicopter Society, Phoenix, Arizona, May 1991.

14. Callahan, C.B. and Straub, F.K.,"Design Optimization of Rotor Blades for Improved Performance and Vibration," Proceedings of the 47th Annual forum of American Helicopter Society, Phoenix, Arizona, May 1991.

15. He, Chengjian and Peters, D.A., "Optimum Rotor Interdisciplinary Design with a Finite State Aeroelastic System," *Computer and Mathematics with Application*, Vol. 17a No.1, 1993.

16. Blackwell, R.H.,"Blade Design for Reduced Helicopter Vibration," American Helicopter Society National Specialists' Meeting on Helicopter Vibration, Hartford, Connecticut, Nov 1981.

17. Gupta, B.P.,"Blade Design Parameters which Affect Helicopter Vibrations," Proceedings of the 40th Annual Forum of American Helicopter Society, Arlington,

Virginia, May 1984.

18. Heffernen, G.K., Yamauchi, M. Gaubert and W. Johnson, " Hub Loads Analysis of the SA349/2 Helicopter," Journal of the American Helicopter Society, Vol. 35, No. 1, January 1990.

19. Johnson, Wayne, "A Comprehensive Analytical Model of Rotorcraft Aerodynamics and Dynamics," Johnson Aeronautics Version, Vol I: Theory Manual, Johnson Aeronautics, Palo Alto, California, 1988.

20. Noonan, K.W., "Aerodynamic Characteristics of Two Rotorcraft Airfoils Designed for Application to the Inboard Region of a Main Rotor Blade," NASA TP-3009, AVSCOM TR-90-B-005, July 1990.

21. Bingham, G. J. and Noonan, K.W.,"Two-Dimensional Aerodynamic Characteristics of Three Rotorcraft Airfoils at Mach Numbers from 0.35 to 0.90," NASA TP-2000, AVRADCOM TR-82-B-2, May 1982.

22. Coleman, Robert P., Feingold, Arnold M., and Stempin, Carl W.," Evaluation of the Induced-Velocity Field of an Idealized Helicopter Rotor," NACA ARR L5E10, June 1945.

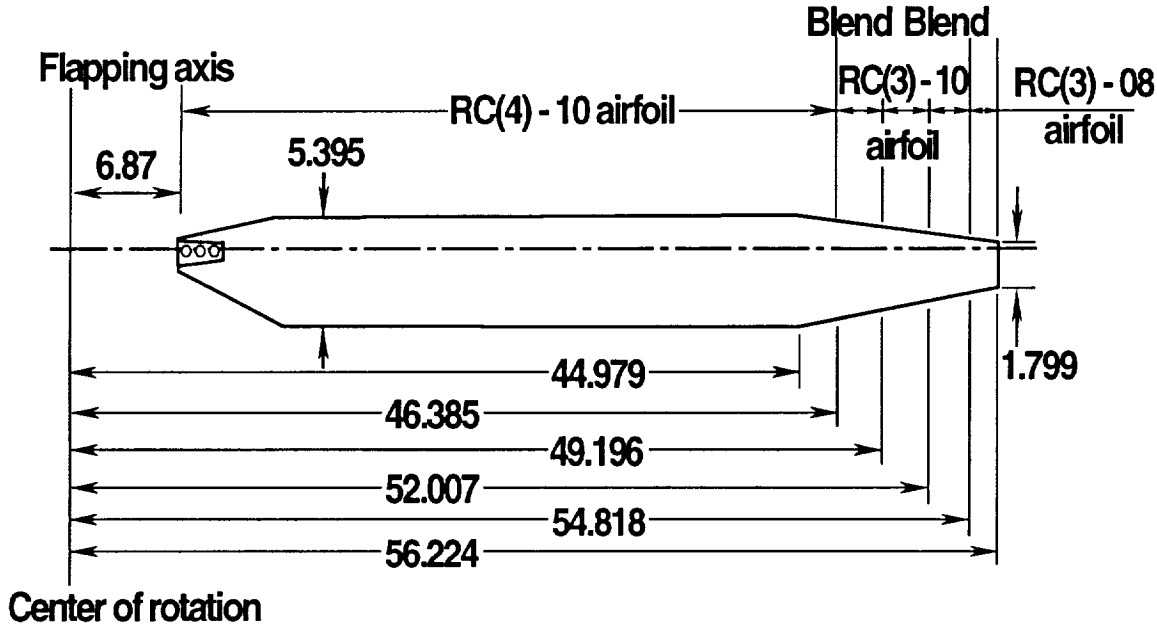

Figure 1 Blade Configuration (in inches)

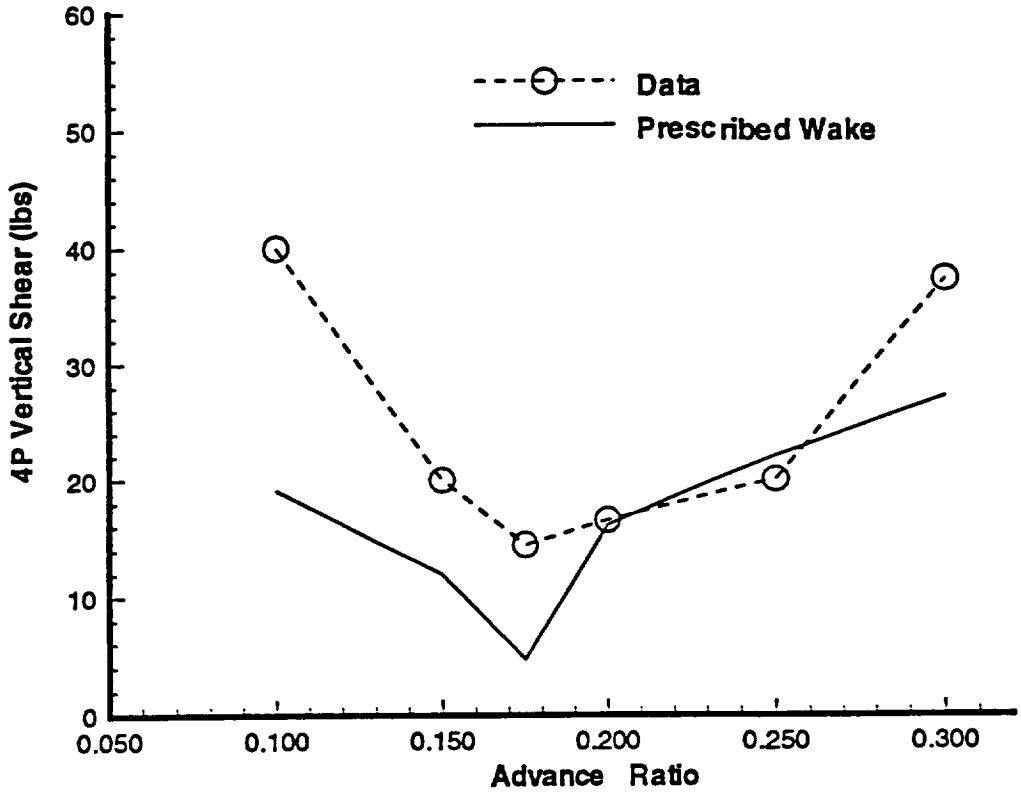

Figure 2 Comparison of theoretical 4P vertical shear with measured data.

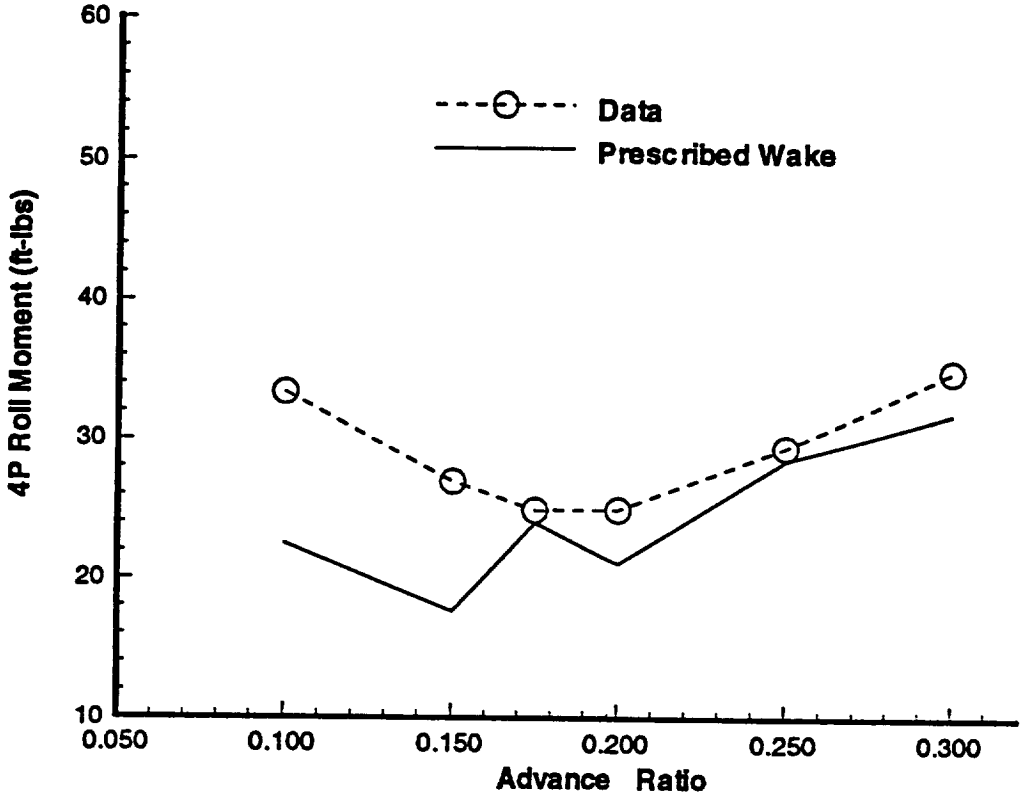

Figure 3 Comparison of theoretical 4P roll moment with measured data.

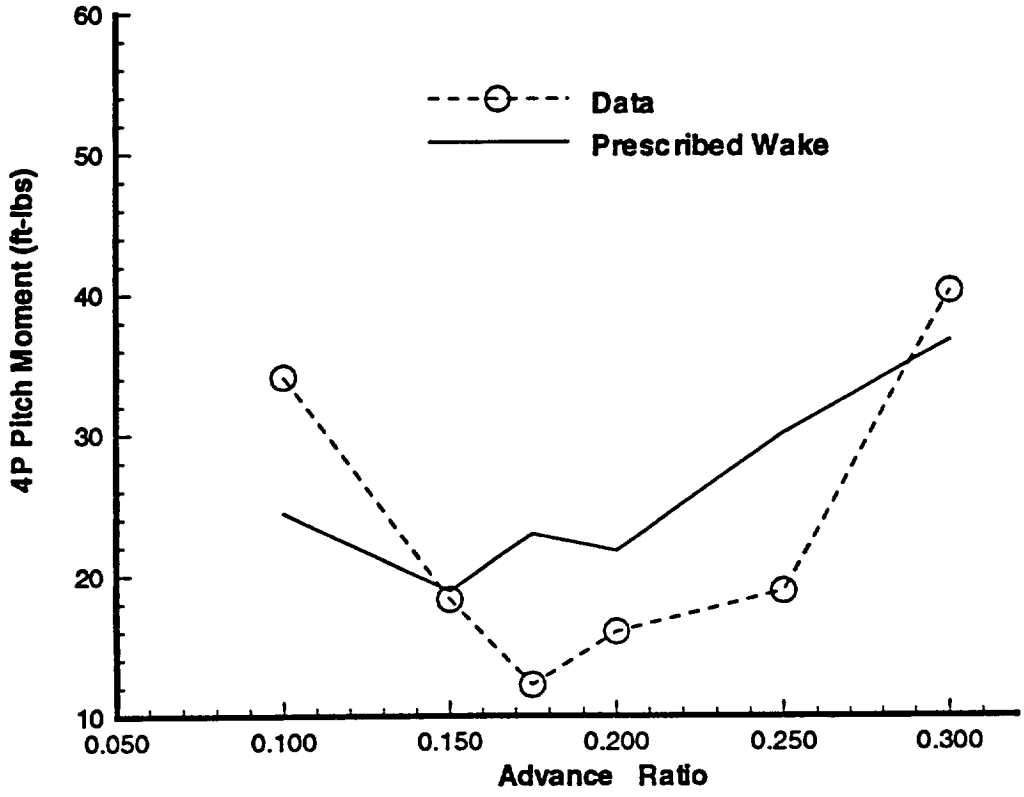

Figure 4 Comparison of theoretical 4P pitch moment with measured data.

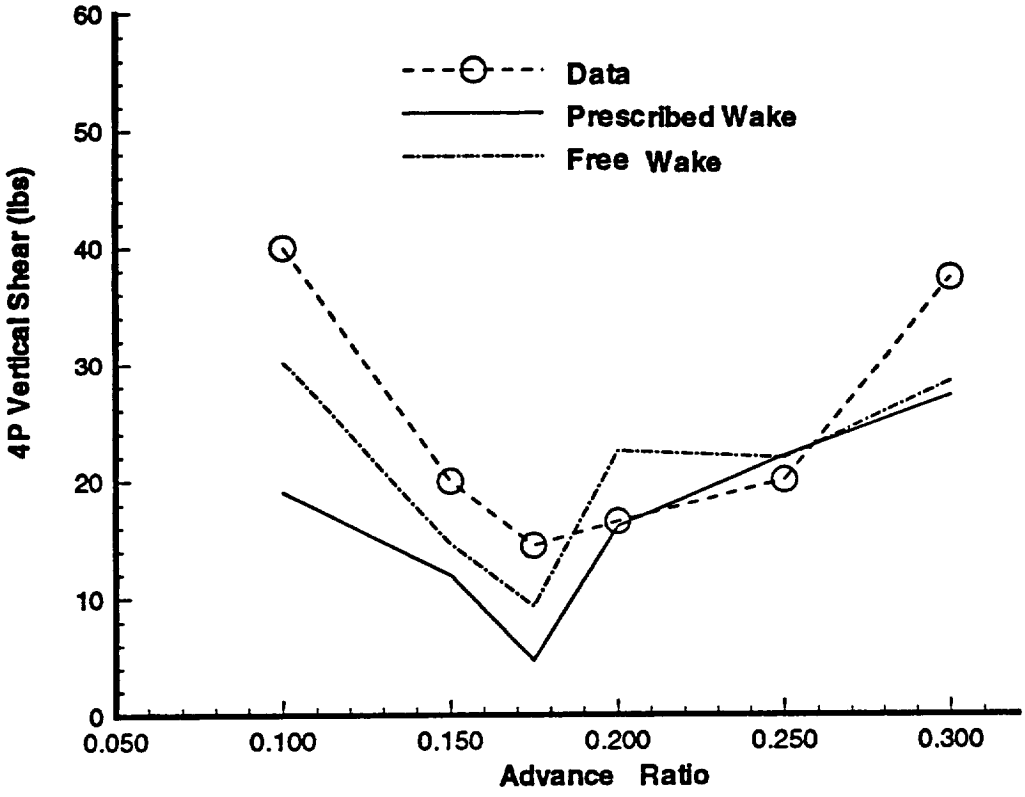

Figure 5 Comparison of prescribed wake and free wake predictions

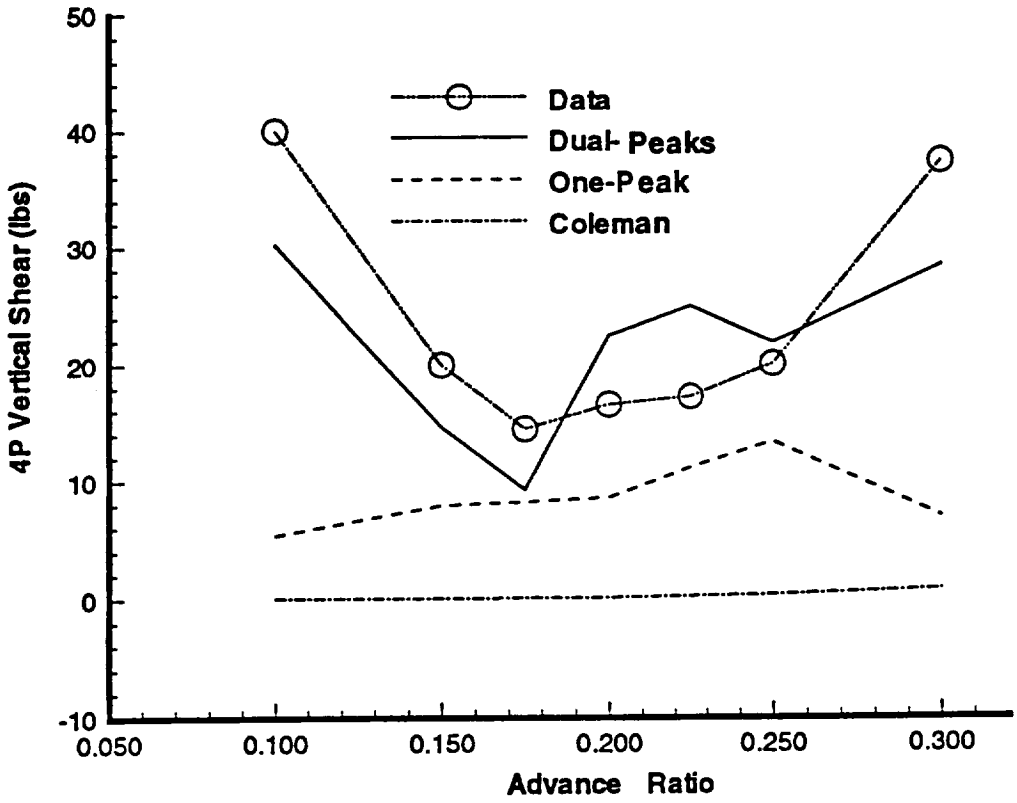

Figure 6 Comparison of different inflow modelings

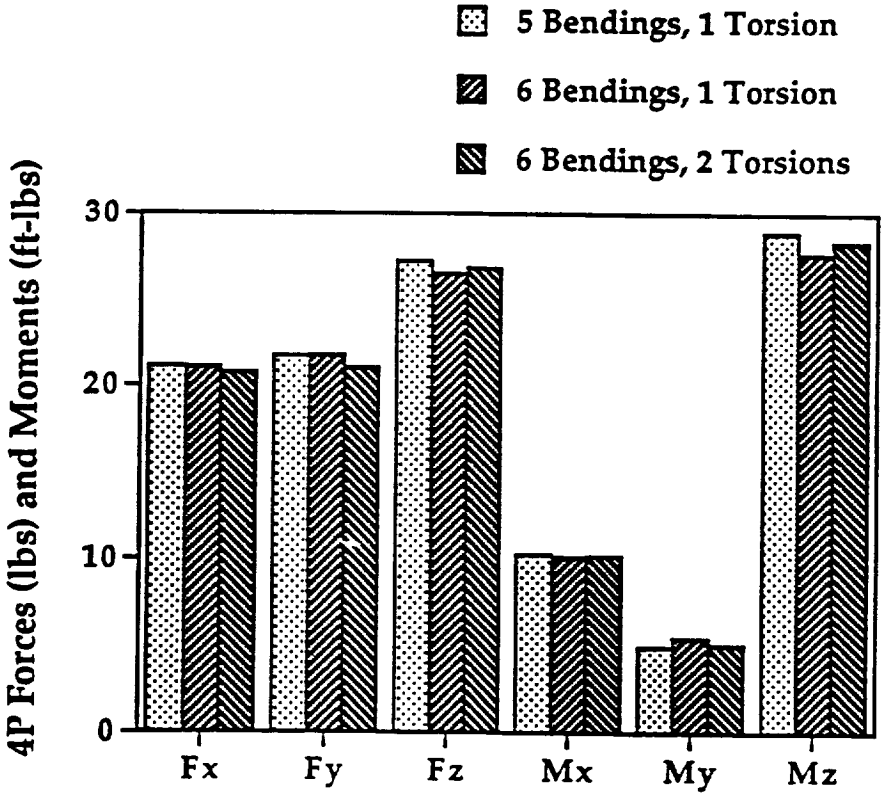

Figure 7 Comparison of blade structural dynamics modeling (μ=0.30).

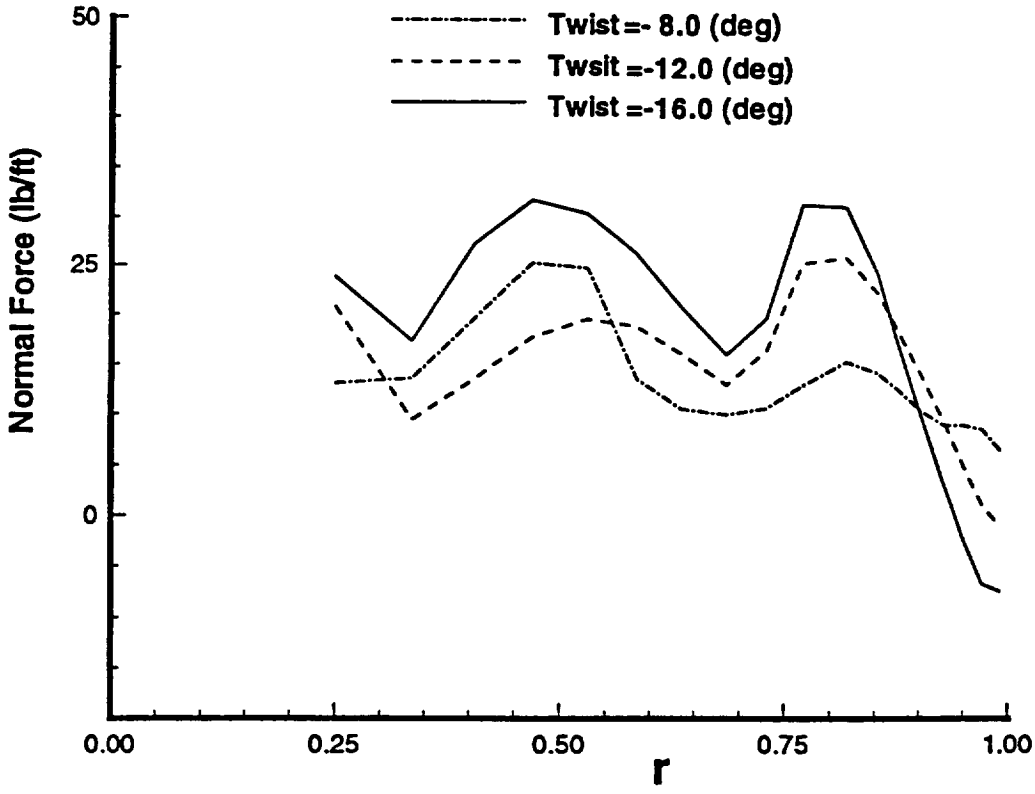

Figure 8 Spanwise variation of sectional normal force, μ=0.30, ψ=90.0 deg.

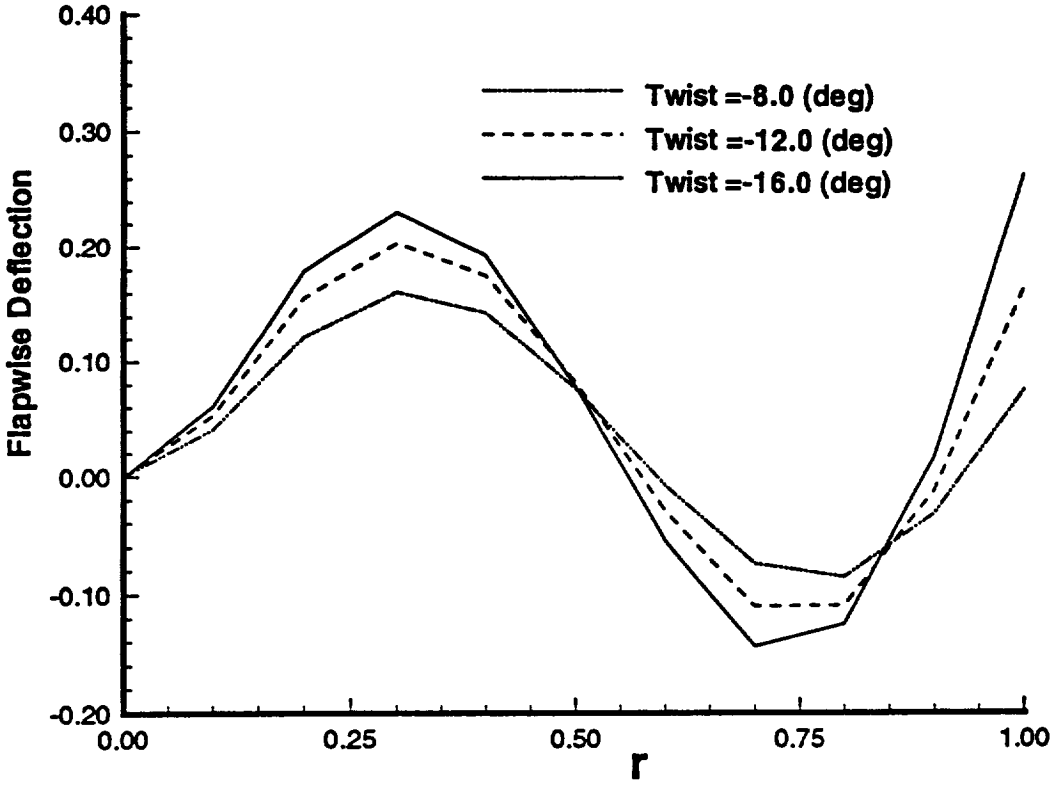

Figure 9 Flapwise deflection of fifth bending mode

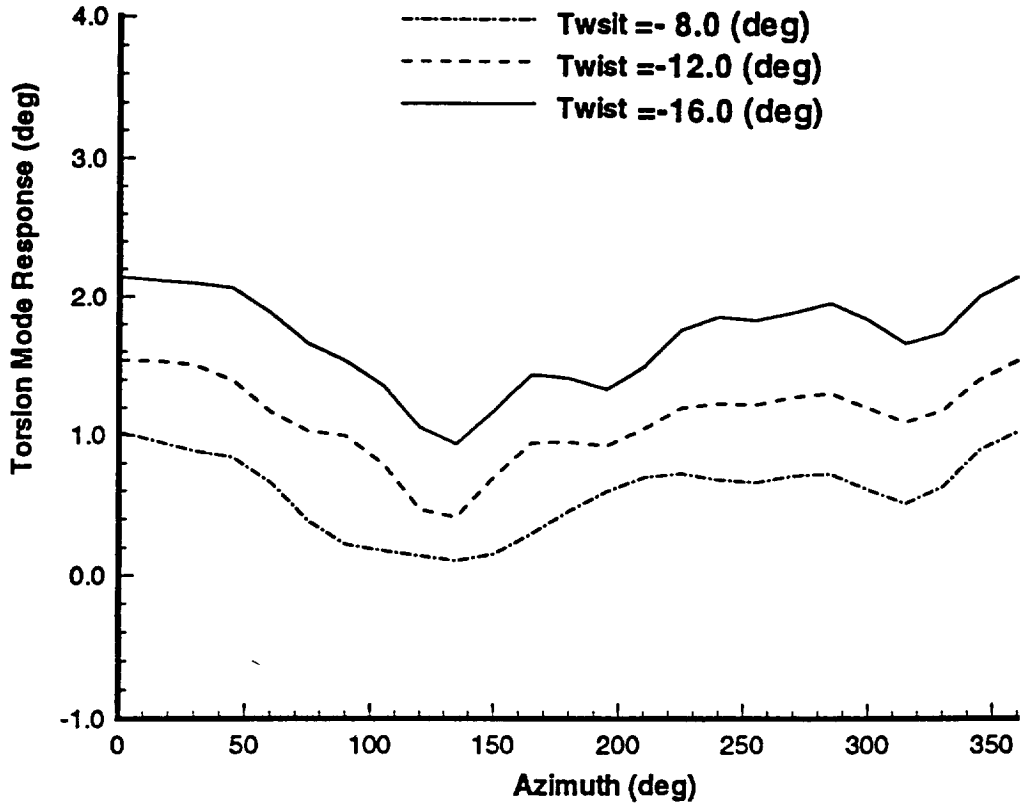

Figure 10 Effect of twist on torsional response

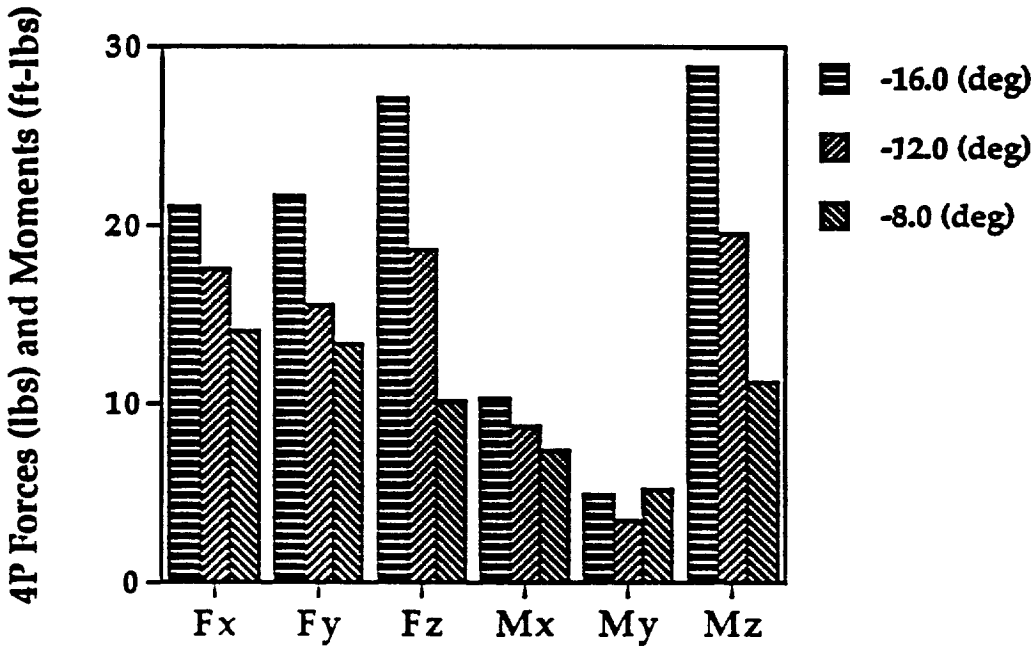

Figure 11 Effect of twist on harmonic hub loads (μ=0.30)

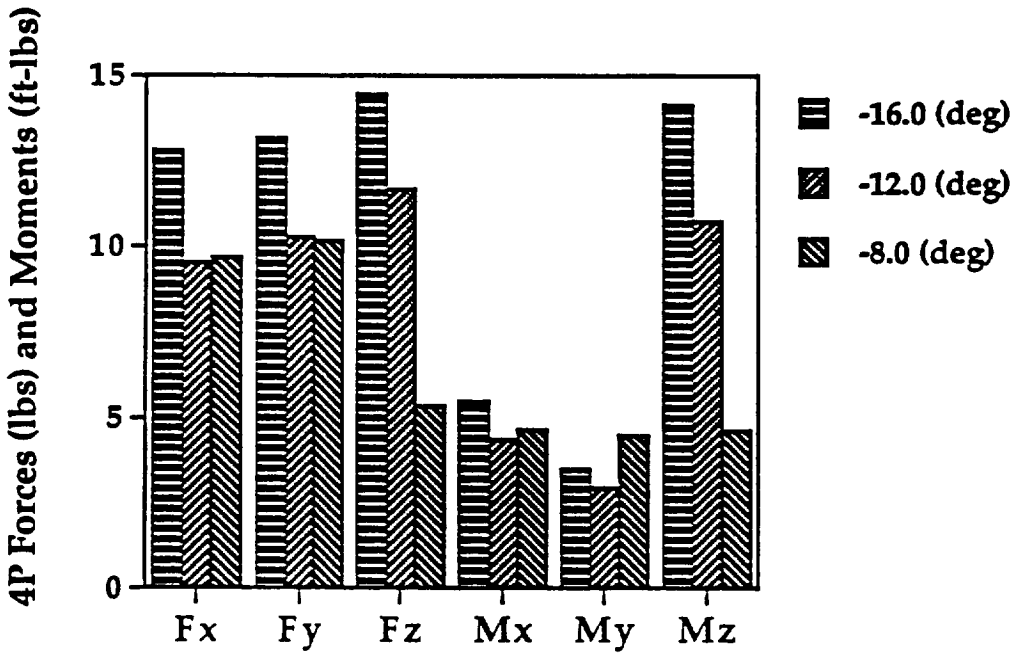

Figure 12 Effect of twist on harmonic hub loads (μ=0.10)

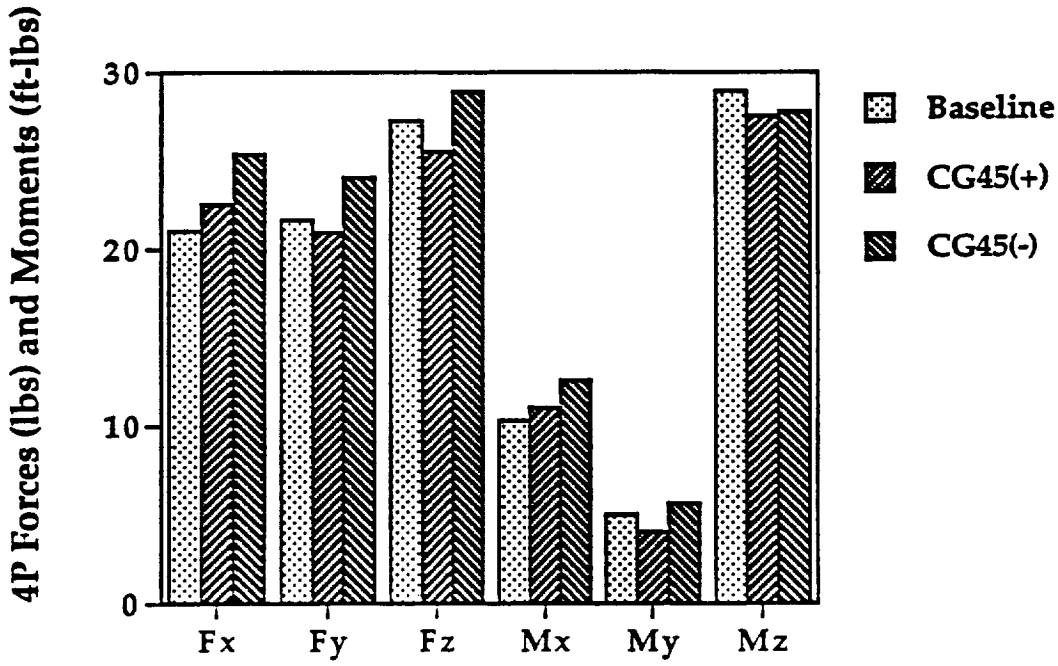

Figure 13 Effect of c.g. offset on harmonic hub loads (μ=0.30)

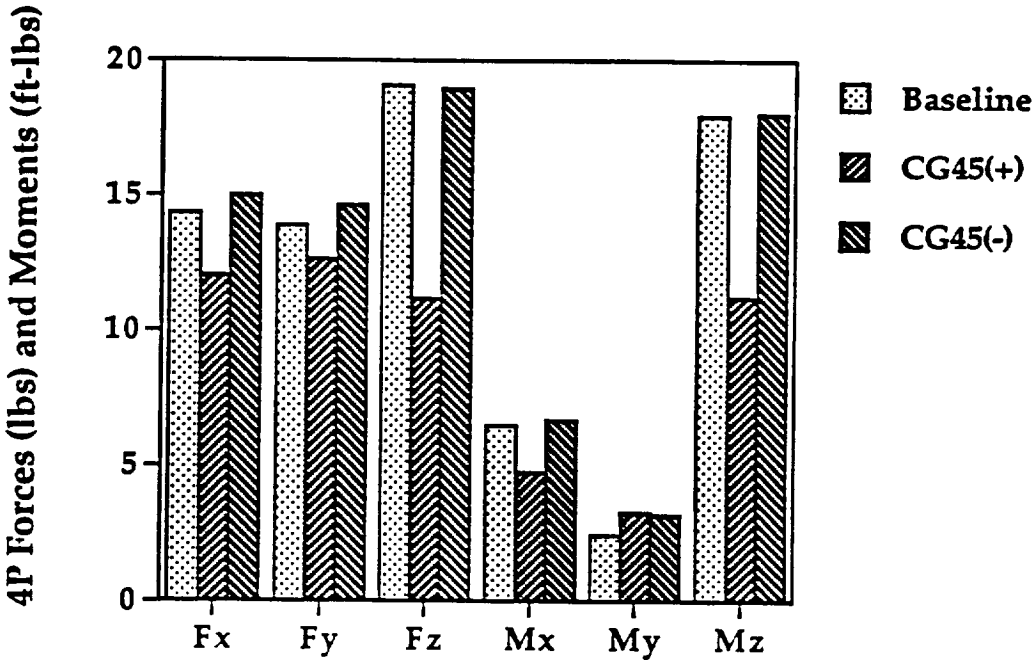

Figure 14 Effect of c.g. offset on harmonic hub loads (μ=0.10)

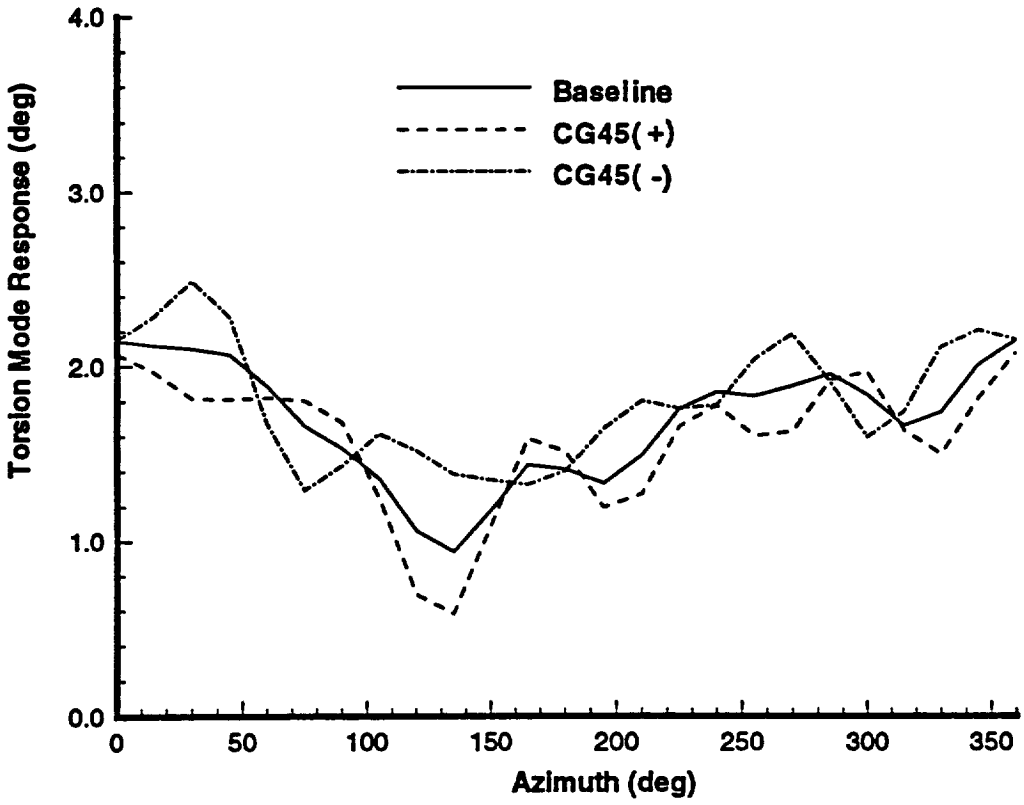

Figure 15 Effect of c.g. offset on torsional response (μ=0.30)

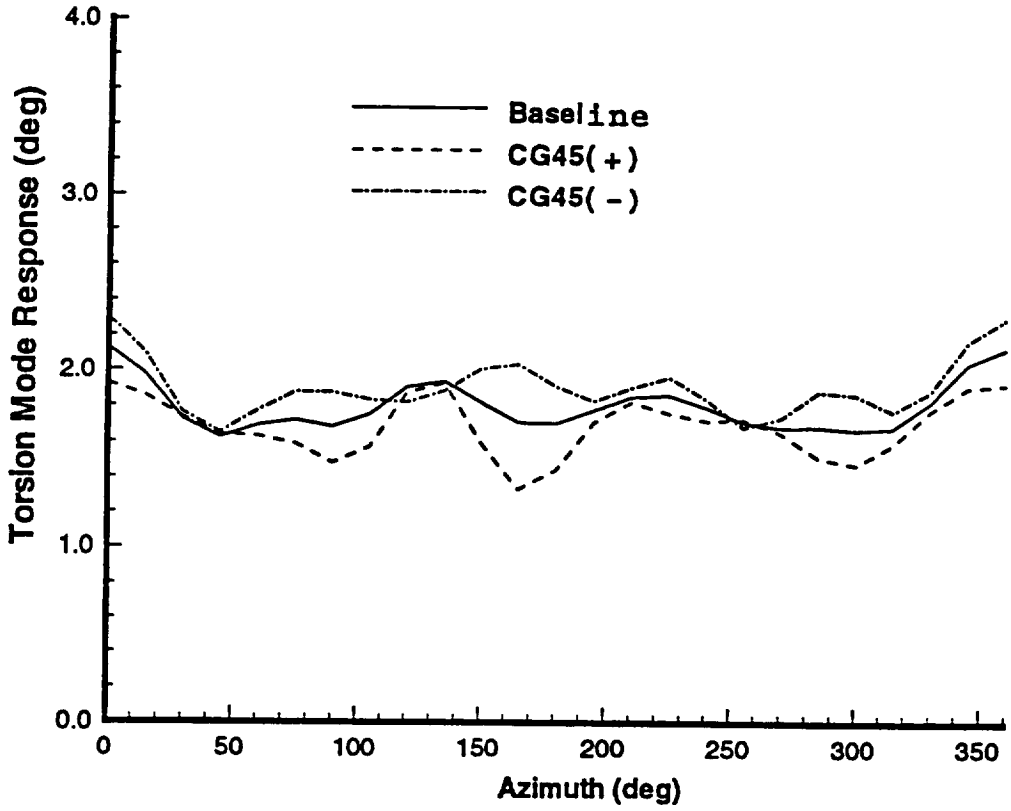

Figure 16 Effect of c.g. offset on torsional response (μ=0.10)

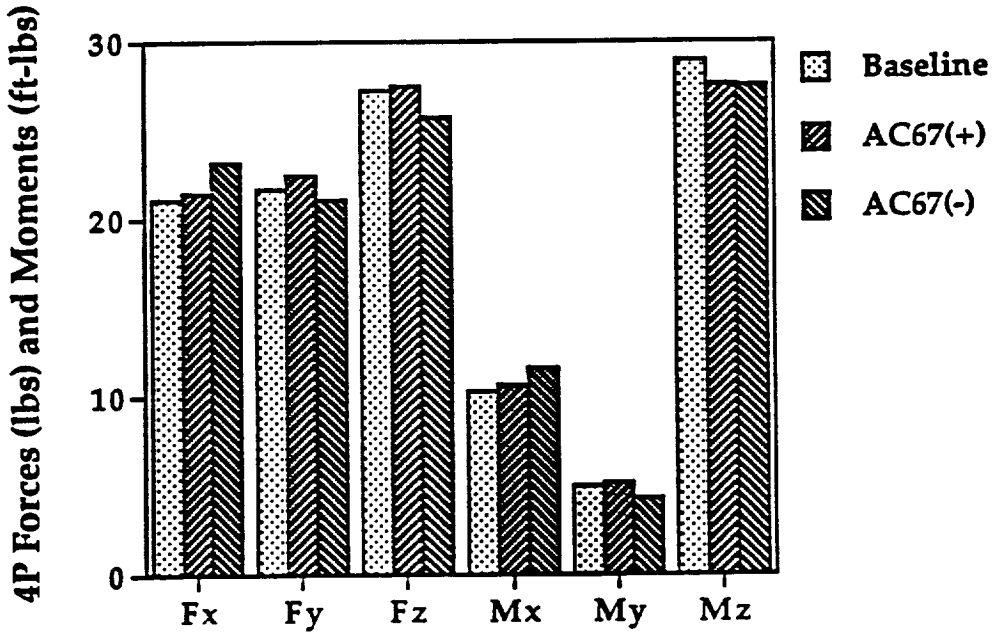

Figure 17 Effect of a.c. offset on harmonic hub loads (μ=0.30)

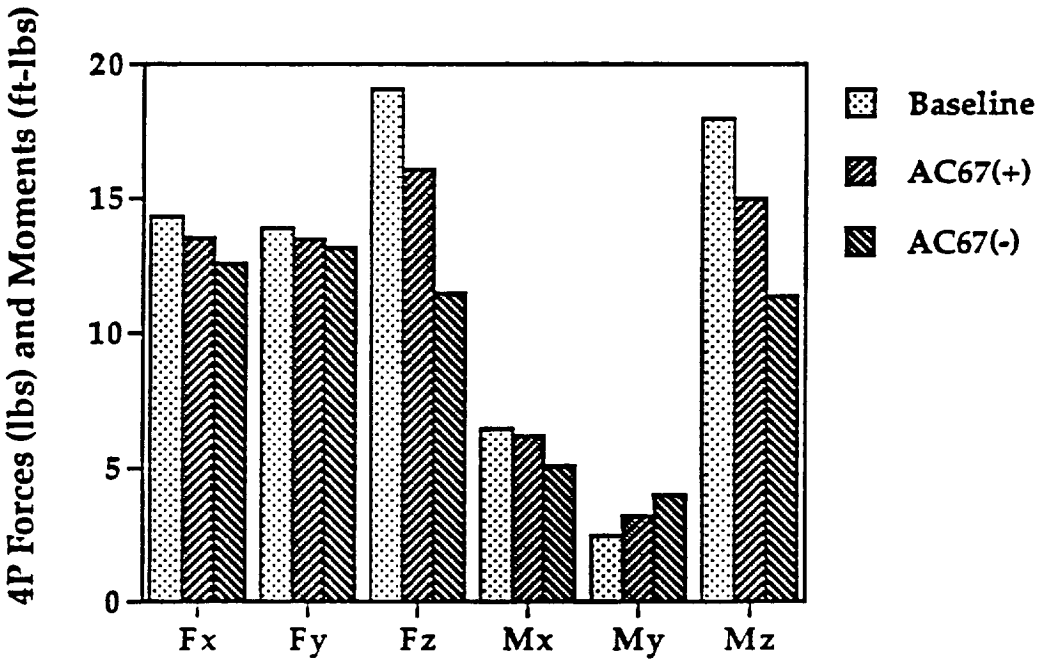

Figure 18 Effect of a.c. offset on harmonic hub loads (μ=0.10)

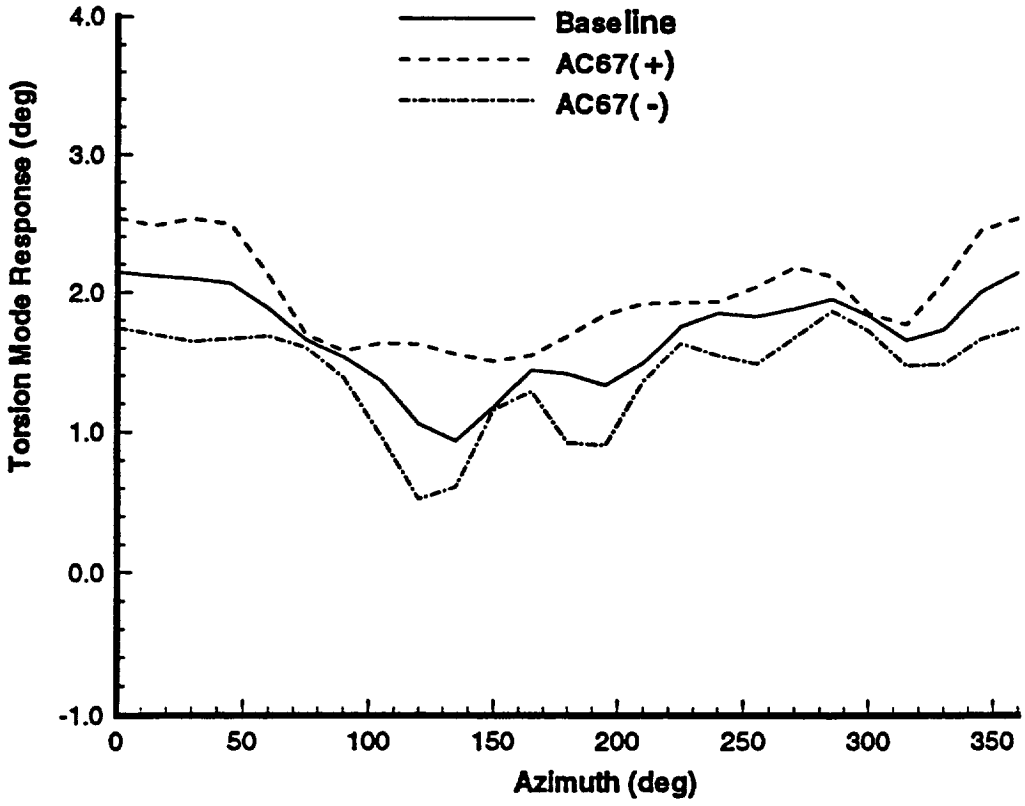

Figure 19 Effect of a.c. offset on torsional response (μ=0.30)

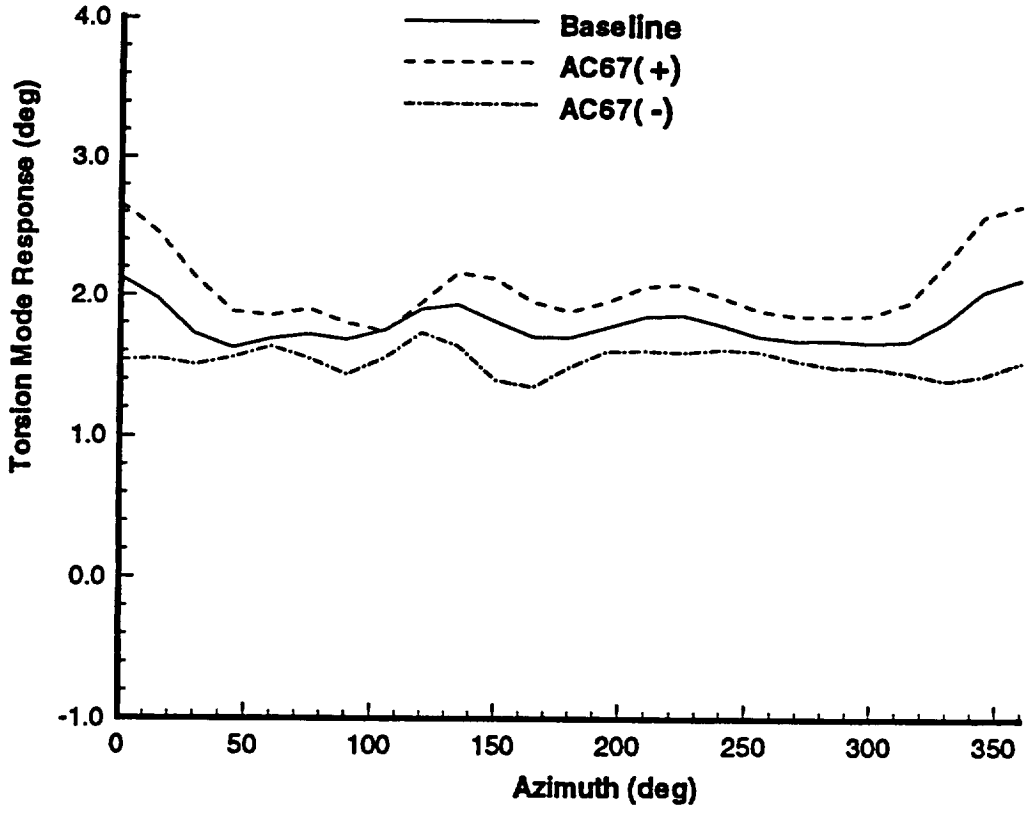

Figure 20 Effect of a.c. offset on torsional response (μ=0.10)

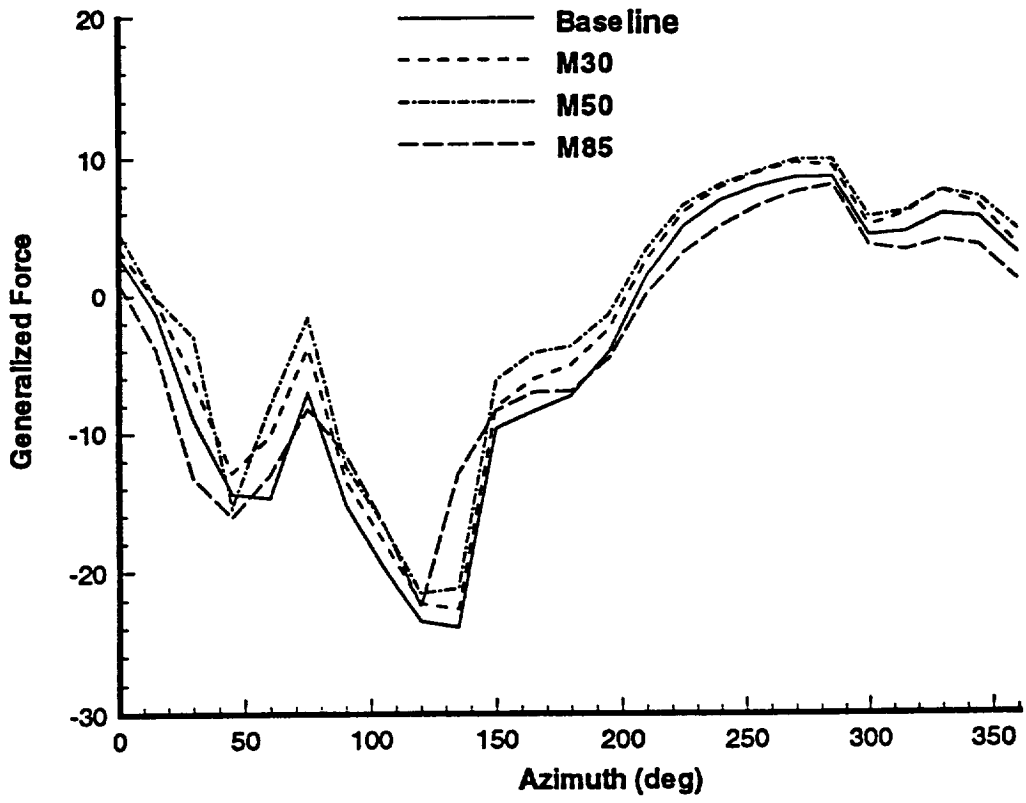

Figure 21 Variation of generalized force of flapwise component of the third mode for different mass tuning configurations (μ=0.30)

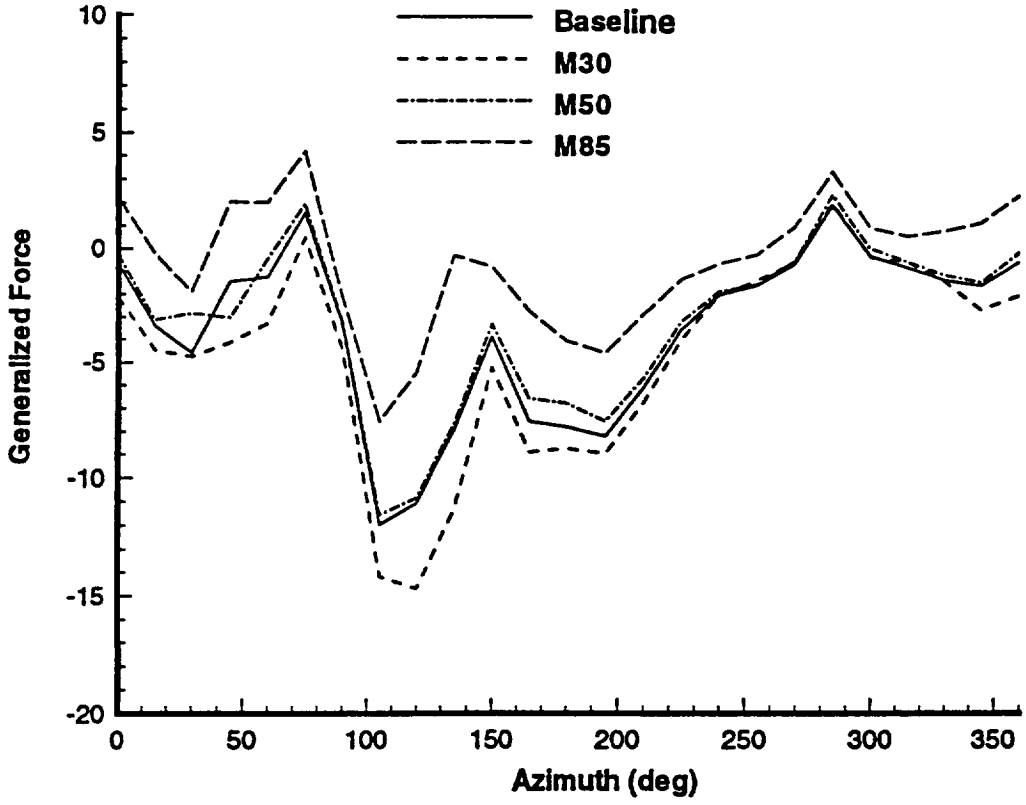

Figure 22 Variation of generalized force of flapwise component of the fourth mode for different mass tuning configurations (μ=0.30)

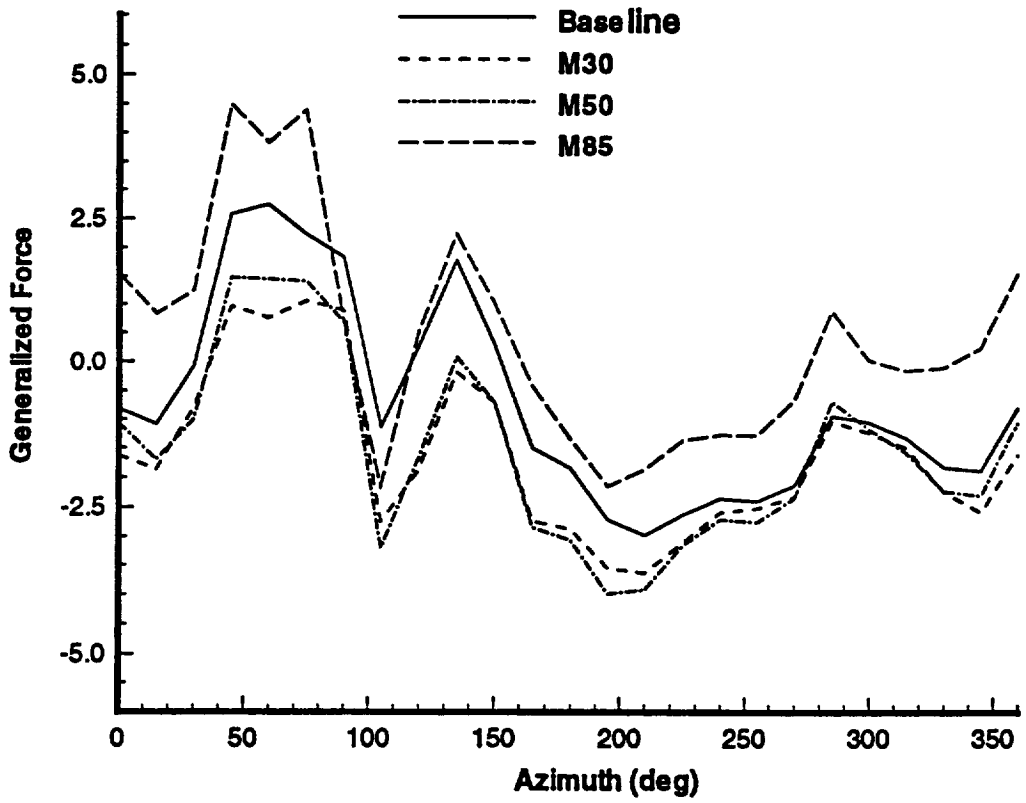

Figure 23 Variation of generalized force of flapwise component of the fifth mode for different mass tuning configurations (μ=0.30)

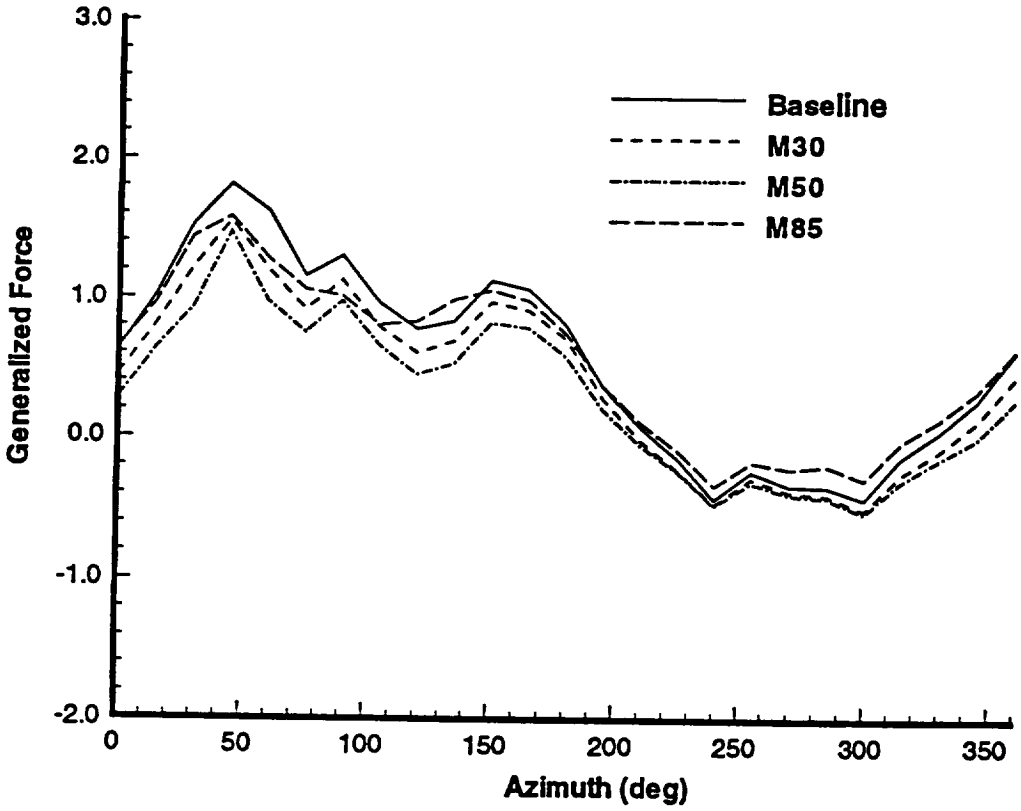

Figure 24 Variation of generalized force of in-plane component of the fifth mode for different mass tuning configurations (μ=0.30)

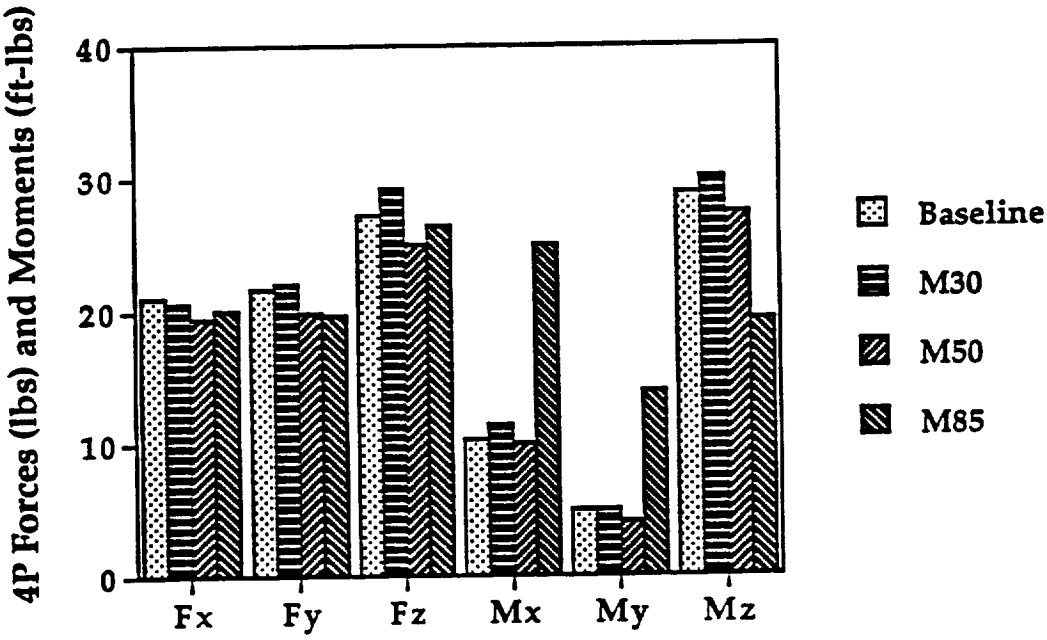

Figure 25 Prediction of effect of addition of mass on harmonic hub loads (μ=0.30)

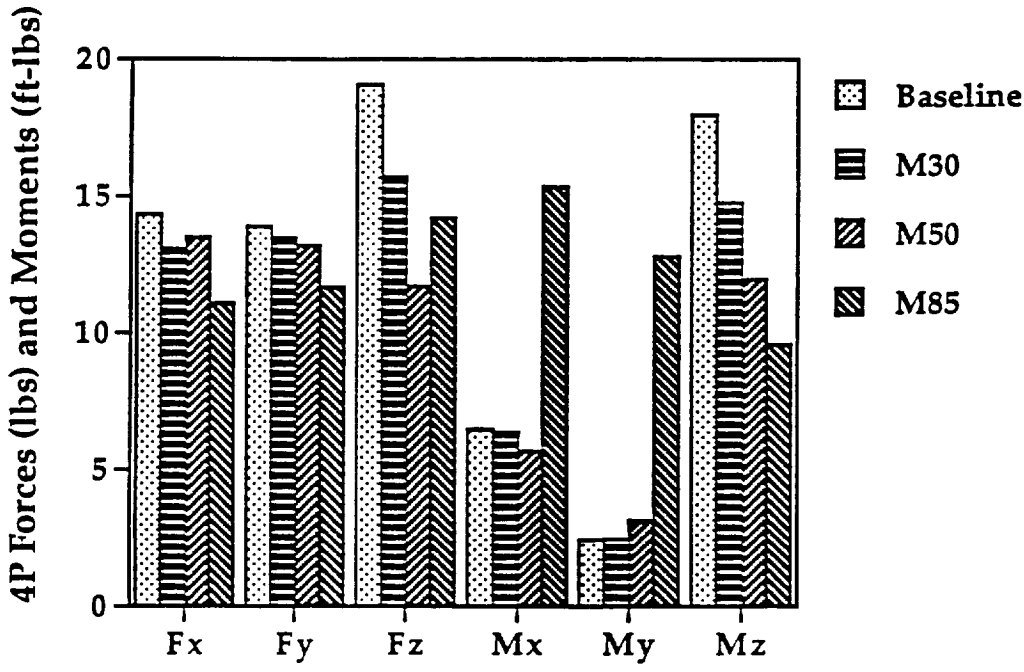

Figure 26 Prediction of effect of addition of mass on harmonic hub loads (μ=0.10)

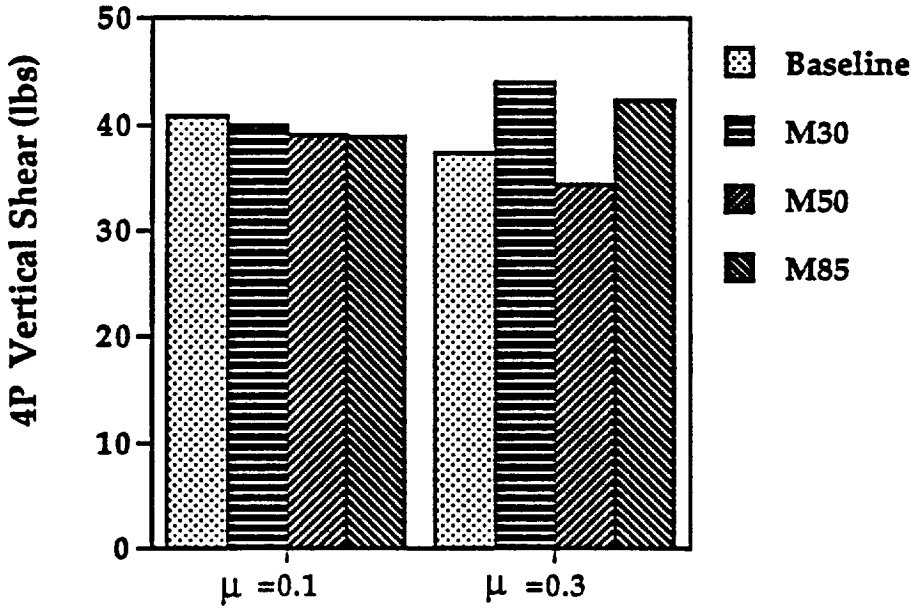

Figure 27 Measurement of effect of addition of mass on 4P vertical shear.

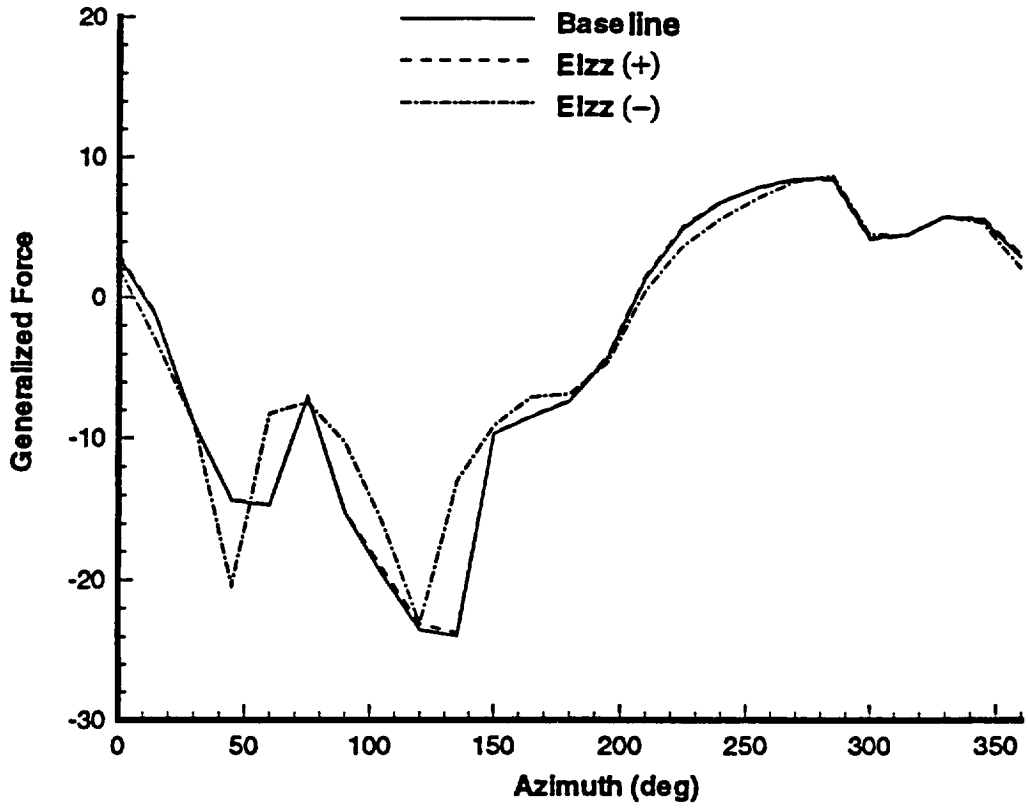

Figure 28 Variation of generalized force of flapwise component of the third mode for flapwise bending stiffness changes (μ=0.30).

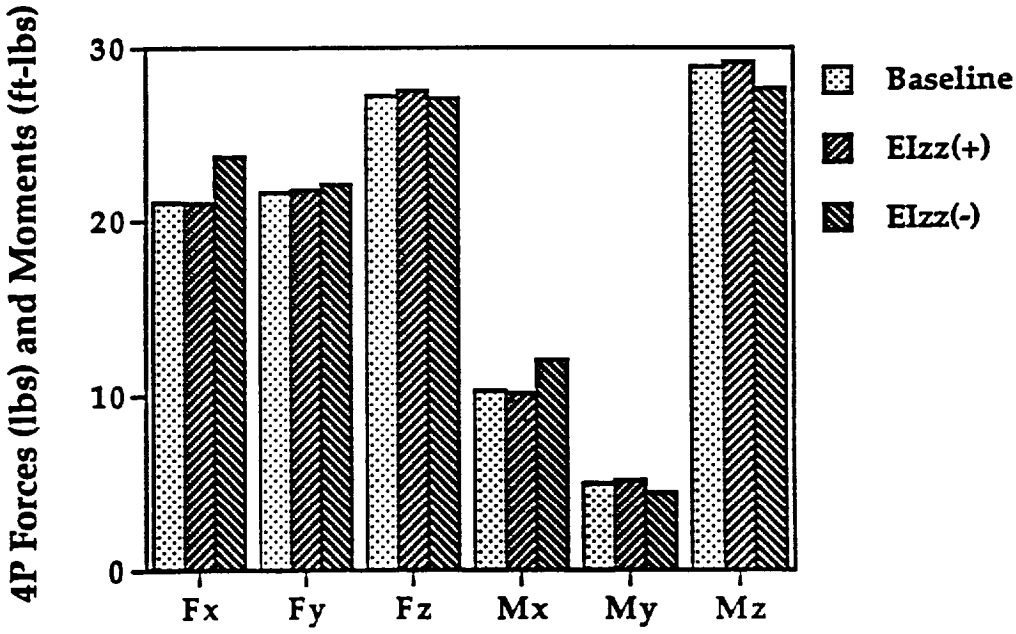

Figure 29 Effect of flapwise bending stiffness on harmonic hub loads (μ=0.30).

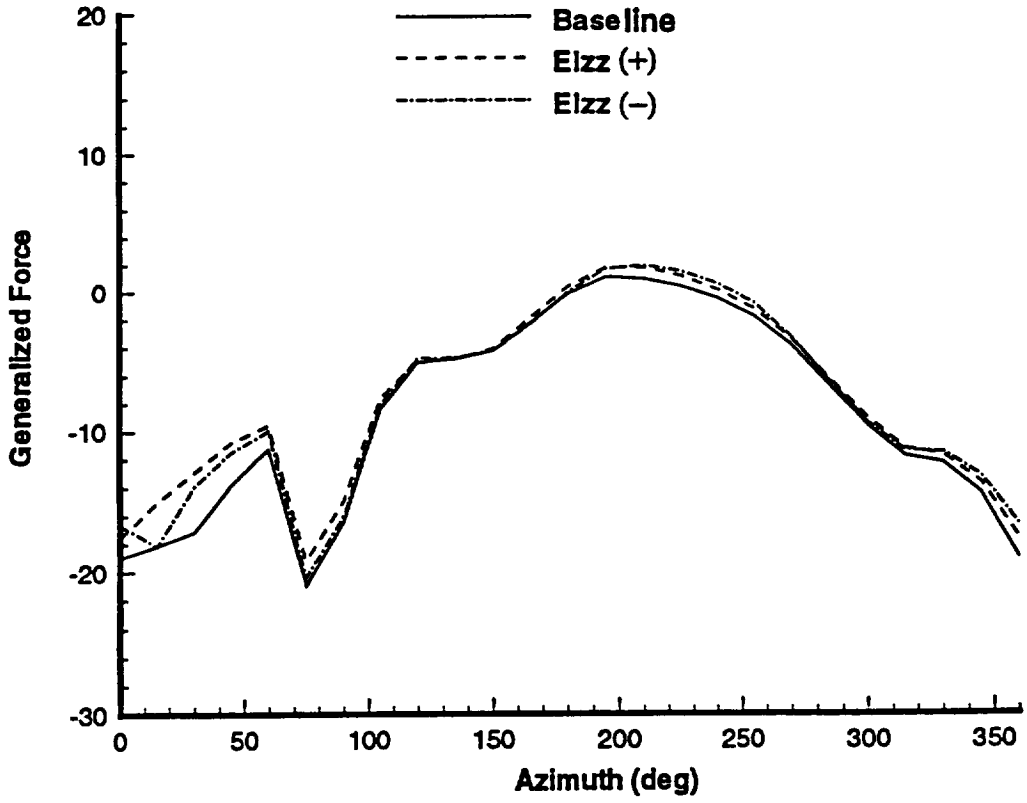

Figure 30 Variation of generalized force of flapwise component of the third mode for flapwise bending stiffness changes (μ=0.10).

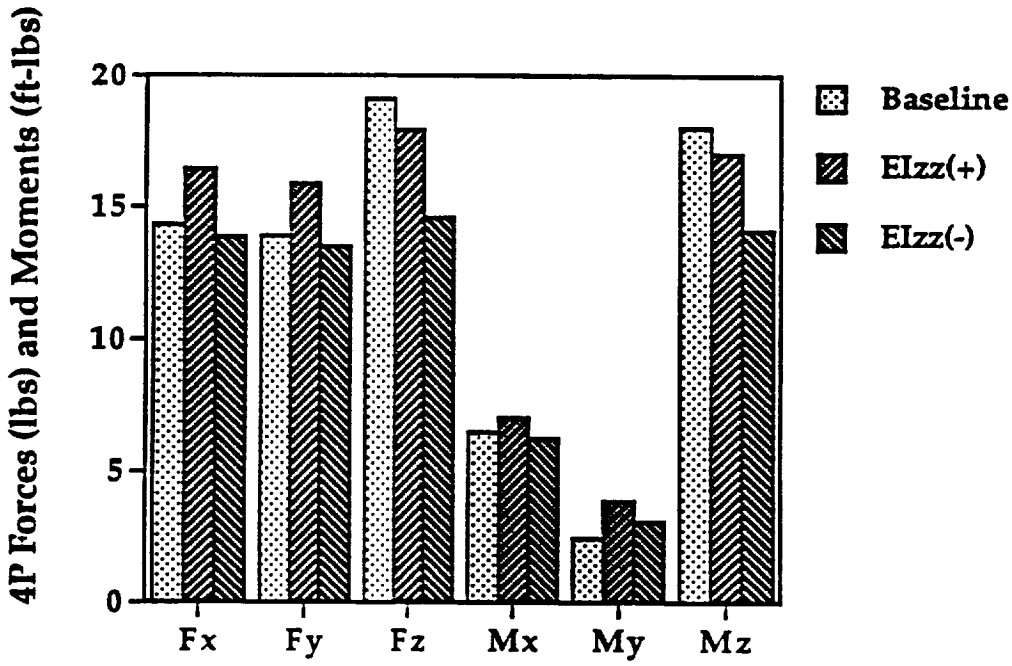

Figure 31 Effect of flapwise bending stiffness on harmonic hub loads (μ=0.10).

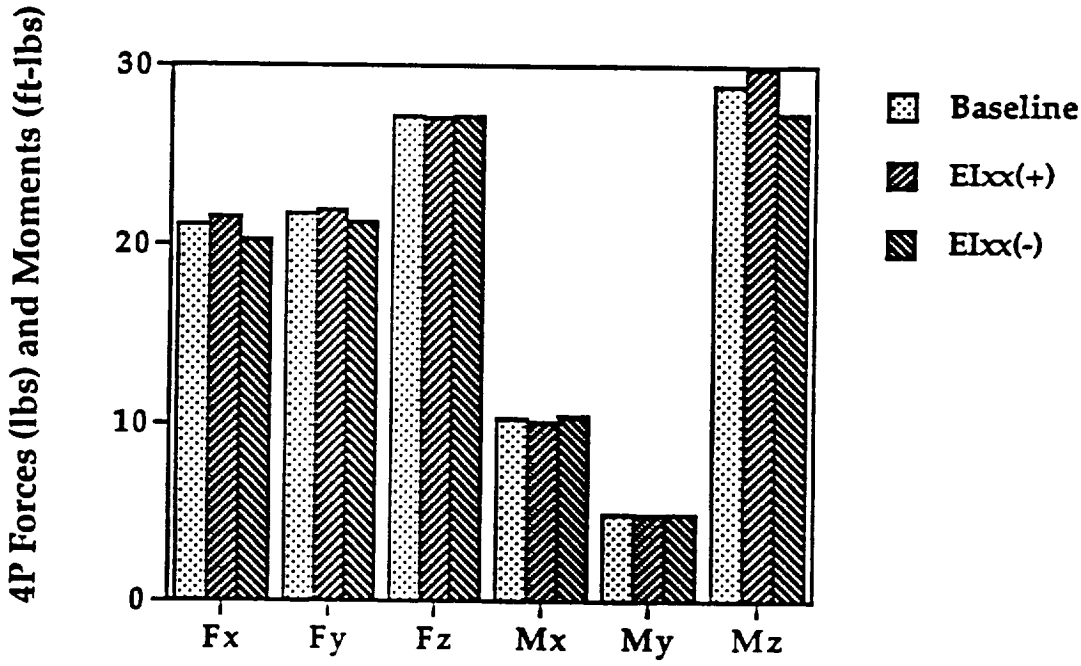

Figure 32 Effect of chordwise bending stiffness on harmonic hub loads (μ=0.30).

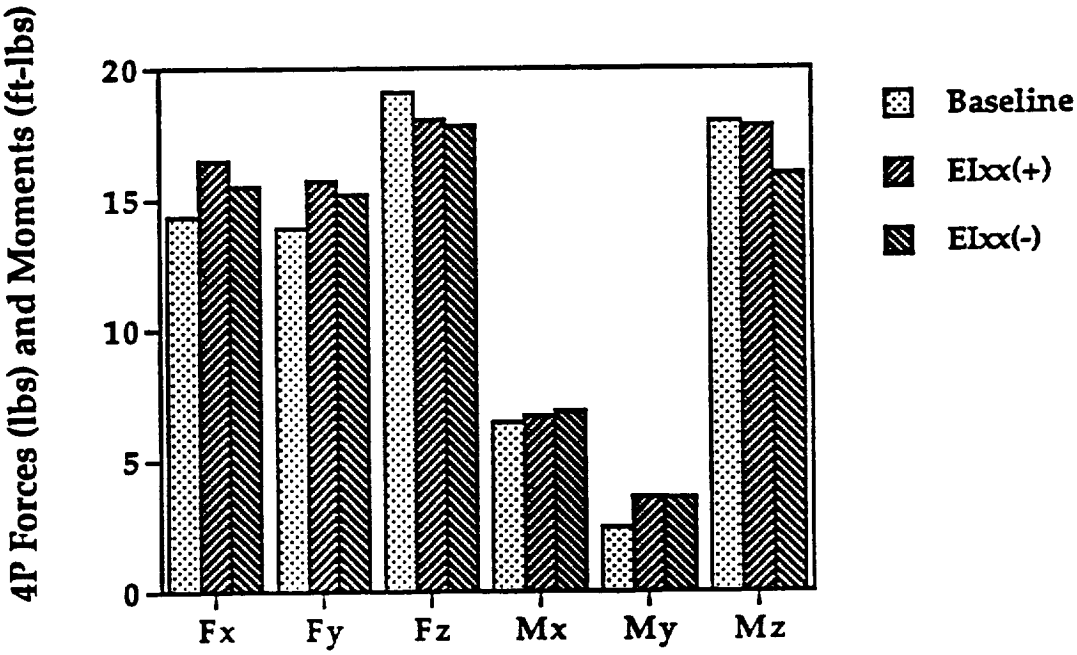

Figure 33 Effect of chordwise bending stiffness on harmonic hub loads (μ=0.10).

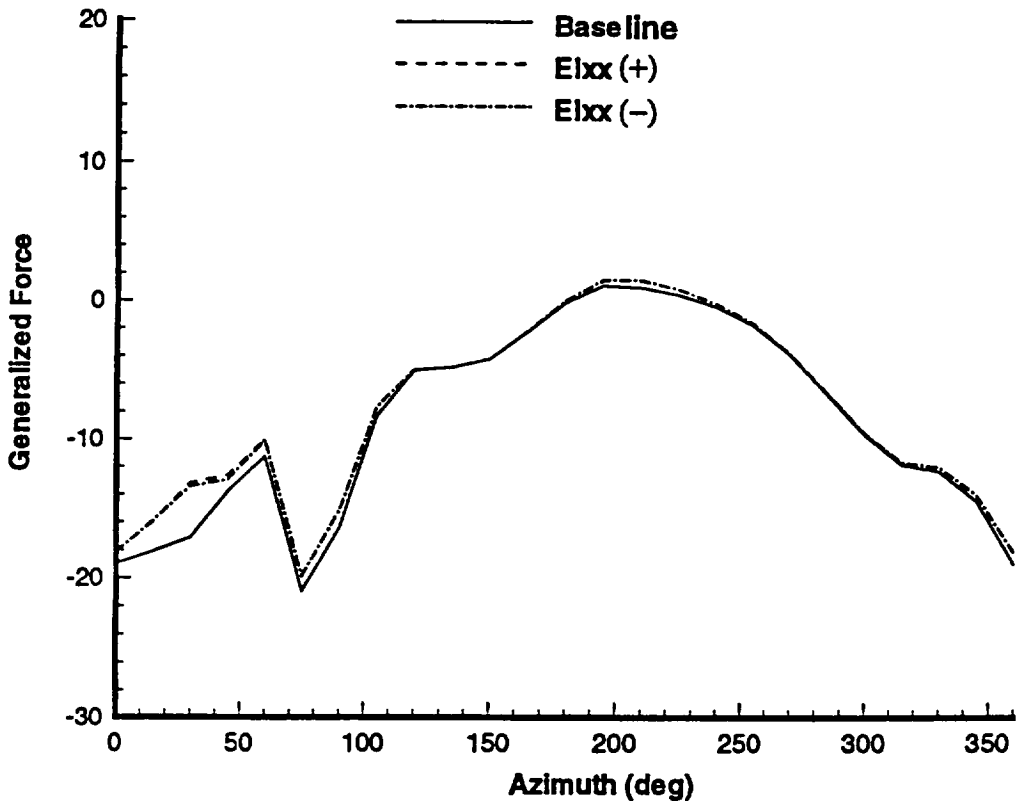

Figure 34 Variation of generalized force of flapwise component of the third mode for chordwise bending stiffness changes (μ=0.10).

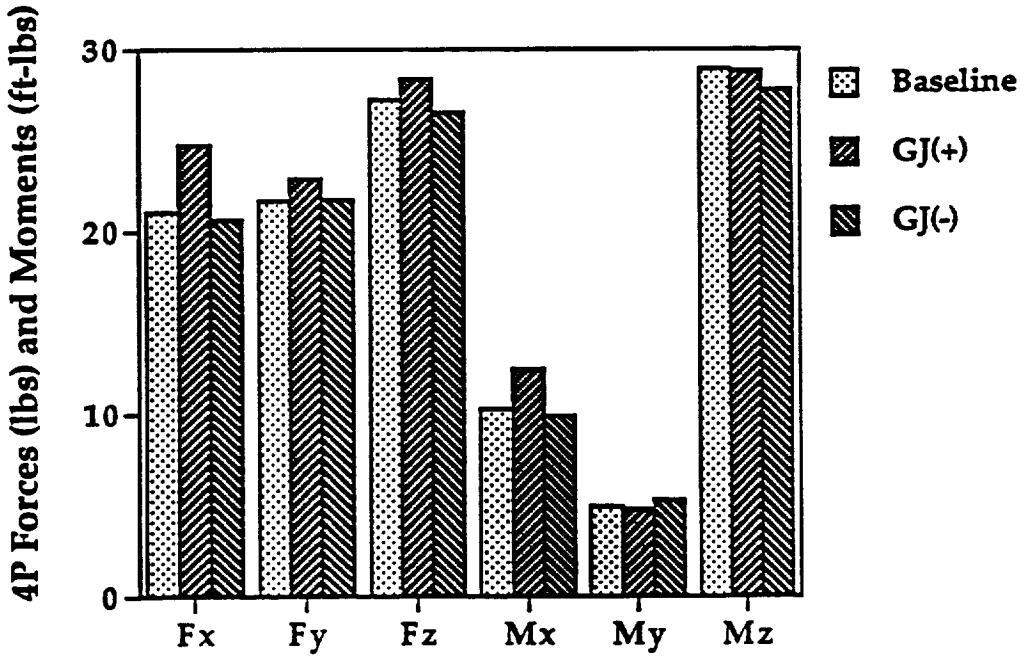

Figure 35 Effect of torsional stiffness on harmonic hub loads (μ=0.30).

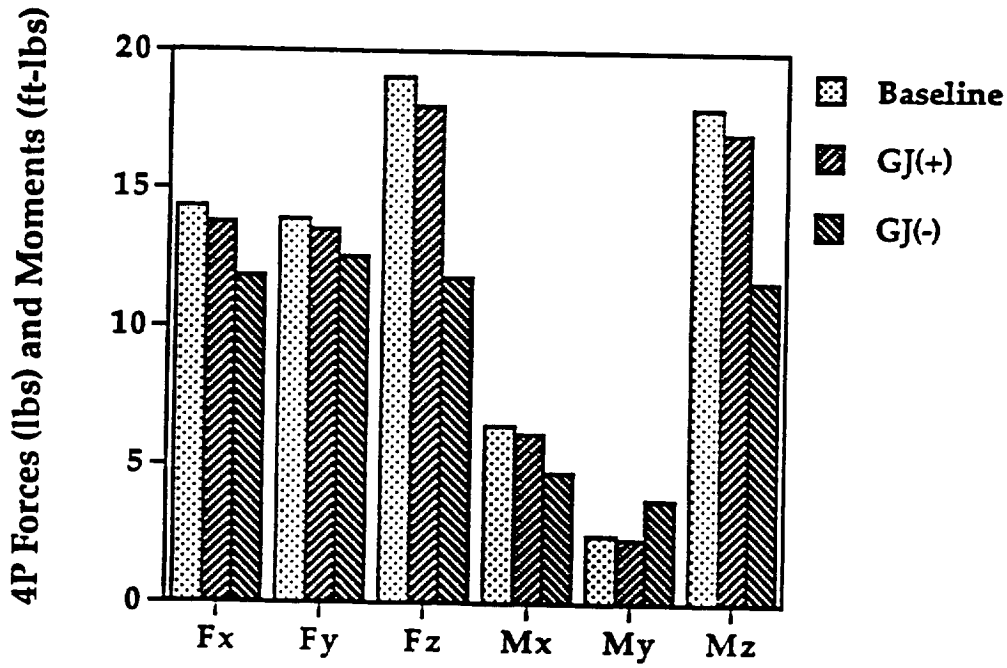

Figure 36 Effect of torsional stiffness on harmonic hub loads (μ=0.10).

REPORT DOCUMENTATION PAGE

Form Approved
OMB No. 0704-0188

1. AGENCY USE ONLY *(Leave blank)*	2. REPORT DATE	3. REPORT TYPE AND DATES COVERED
	November 1993	Contractor Report

4. TITLE AND SUBTITLE
A Parametric Study of Harmonic Rotor Hub Loads

5. FUNDING NUMBERS
C NAS1-19000
WU 505-63-36

6. AUTHOR(S)
Chengjian He

7. PERFORMING ORGANIZATION NAME(S) AND ADDRESS(ES)
Lockheed Engineering & Sciences Co.
144 Research Drive
Hampton, VA 23666

8. PERFORMING ORGANIZATION REPORT NUMBER

9. SPONSORING / MONITORING AGENCY NAME(S) AND ADDRESS(ES)
NASA Langley Research Center
Hampton, VA 23681-0001

10. SPONSORING / MONITORING AGENCY REPORT NUMBER
NASA CR-4558

11. SUPPLEMENTARY NOTES
Langley Technical Monitor: Jaroslaw Sobieski

12a. DISTRIBUTION / AVAILABILITY STATEMENT
Unclassified - Unlimited

Subject Category 05

12b. DISTRIBUTION CODE

13. ABSTRACT *(Maximum 200 words)*

This report presents a parametric study of vibratory rotor hub loads in a nonrotating system. The study is based on a CAMRAD/JA model constructed for the GBH (Growth Version of Blackhawk Helicopter) Mach-scaled wind tunnel rotor model with high blade twist (-16°). The theoretical hub load predictions are validated by correlation with available measured data. Effects of various blade aeroelastic design changes on the harmonic nonrotating frame hub loads at both low and high forward flight speeds are investigated. The study aims to illustrate some of the physical mechanisms for change in the harmonic rotor hub loads due to blade design variations.

14. SUBJECT TERMS
Blade Dynamics
Rotor Aeroelatic Response
Rotor Aerodynamics

15. NUMBER OF PAGES
64

16. PRICE CODE
A04

17. SECURITY CLASSIFICATION OF REPORT	18. SECURITY CLASSIFICATION OF THIS PAGE	19. SECURITY CLASSIFICATION OF ABSTRACT	20. LIMITATION OF ABSTRACT
Unclassified	Unclassified	Unclassified	Unlimited